AGU PUBLICATIONS

Space Weather

REVIEW ARTICLE
10.1002/2014SW001060

Key Points:
- It presents an overall review on the CME/shock arrival time predictions
- It outlines the principle of each model
- It discusses the further direction of CME/shock arrival time prediction

Correspondence to:
M. Dryer,
murraydryer@msn.com

Citation:
Zhao, X., and M. Dryer (2014), Current status of CME/shock arrival time prediction, *Space Weather*, *12*, 448–469, doi:10.1002/2014SW001060.

Received 26 FEB 2014
Accepted 3 JUN 2014
Accepted article online 9 JUN 2014
Published online 1 JUL 2014

Current status of CME/shock arrival time prediction

Xinhua Zhao[1] and Murray Dryer[2]

[1]SIGMA Weather Group, State Key Laboratory of Space Weather, Center for Space Science and Applied Research, Chinese Academy of Sciences, Beijing, China, [2]Emeritus, Space Weather Predictions Center, National Weather Service, National Oceanic and Atmospheric Administration, Boulder, Colorado, USA

Abstract One of the major solar transients, coronal mass ejections (CMEs) and their related interplanetary shocks have severe space weather effects and become the focus of study for both solar and space scientists. Predicting their evolutions in the heliosphere and arrival times at Earth is an important component of the space weather predictions. Various kinds of models in this aspect have been developed during the past decades. In this paper, we will present a view of the present status (during Solar Cycle 24 in 2014) of the space weather's objective to predict the arrival of coronal mass ejections and their interplanetary shock waves at Earth. This status, by implication, is relevant to their arrival elsewhere in the solar system. Application of this prediction status is clearly appropriate for operational magnetospheric and ionospheric situations including A −> B −> C…solar system missions. We review current empirical models, expansion speed model, drag-based models, physics-based models (and their real-time prediction's statistical experience in Solar Cycle 23), and MHD models. New observations in Solar Cycle 24, including techniques/models, are introduced as they could be incorporated to form new prediction models. The limitations of the present models and the direction of further development are also suggested.

1. Introduction

Coronal mass ejections (CMEs), as one of the most violent forms of solar activity, refer to large-scale eruptions of plasma and magnetic field that erupt from the Sun and propagate into interplanetary space [*Hundhausen et al.*, 1984; *Hudson et al.*, 2006]. Typical CMEs propagate outward at the speed of 200–3000 km/s, carry the mass of even 10^{12} kg, and therefore possess the kinematic energy exceeding 10^{25} J. The occurrence frequency of CMEs is about 1 CME per several days during solar activity minimum, while it becomes several CMEs per day during solar activity maximum. Shortly after their discovery in the 1970s, CMEs have attracted close attention and extensive studies from both solar and space scientists and are believed to be the major sources to drive the severe space weather events. On one hand, CMEs can produce nonrecurrent geomagnetic storms when colliding with the Earth's magnetosphere if they contain a strong and sustained southward magnetic field component [*Sheeley et al.*, 1985; *Gosling et al.*, 1991]. On the other hand, fast CMEs propagating in solar wind will drive an interplanetary shock, which plays a dominant role in generating large solar energetic particle (SEP) events [*Gopalswamy et al.*, 2003; *Cliver and Ling*, 2009]. In addition, the Earth-directed CMEs also threaten the safety of spacecraft, communication systems, navigation systems, astronauts, and ground-based technical systems (power grids and pipelines) [*Boteler et al.*, 1998; *Lanzerotti*, 2005; *Zheng et al.*, 2013].

Due to the great significance of CMEs and their interplanetary shocks, in the context of space weather as mentioned above, predicting their arrival times at the Earth's space is a major objective of the various national forecast centers. Generally speaking, it takes CMEs 1–5 days to propagate from the Sun to our Earth's location, which enables the prediction of their arrival times in advance become feasible theoretically. The prediction of CME/shock arrival time means that forecasters utilize the observables of solar disturbance obtained before their arrivals as inputs to predict whether/when they will arrive. The earlier observables are used, the longer lead time that the prediction will yield. The observations of CMEs are usually carried out by coronagraphs onboard spacecraft (for example, Large Angle and Spectrometric Coronagraph (LASCO) onboard SOHO and Sun Earth Connection Coronal and Heliospheric Investigation (SECCHI) onboard STEREO-A/STEREO-B). Observations of this kind, called remote sensing, can provide the kinematic parameters of CMEs, such as their velocity, acceleration, trajectory, and angular width. Another way of remote sensing to track the disturbances of CMEs, especially their related shocks, is radio burst emission. According to the

plasma theory, a shock traveling in the corona and interplanetary medium will produce an emission at the fundamental and/or harmonic frequency of the plasma, f_p, which is directly related to the local plasma density. As the shock propagates from the high-density corona to the low-density interplanetary medium, the local plasma frequency will decrease. This gives rise to a slow drift (type II) radio burst [*Payne-Scott et al.*, 1947]. The drifting speed of the burst provides an estimation of the shock's propagating speed. CMEs are usually referred to as interplanetary CMEs (ICMEs) when they propagate into the interplanetary space. Ground-based interplanetary scintillation (IPS) measurements are also used to track the motion of ICMEs indirectly beyond the field of view (FOV) of coronagraphs [*Manoharan et al.*, 2000]. Recently, ICMEs can also be tracked by coronagraphs of large FOVs, such as Solar Mass Ejection Imager and HI/STEREO, to a relatively large helio-distance. Detailed properties of ICMEs at 1 AU are obtained from in situ measurements of magnetic field and plasma by the passing of spacecraft through them. The observations of ICMEs at 1 AU combined with the observations of CMEs near the Sun allow us to establish a direct association between CMEs and their interplanetary counterparts. Then the arrival time of CMEs at 1 AU can be related to their characteristics (velocity, acceleration, …) at the Sun in order to develop the prediction methods for CME's arrival time [*Owens and Cargill*, 2004]. Many papers have been focused on or involved in the arrival time prediction of CMEs and their related shocks. This paper will give an overall review on the CME/shock disturbance arrival time prediction and their current (2014) prediction status. We will outline the principles of the models in section 2 and discuss the direction of further development on this aspect of CME/shock arrival time prediction. We will not discuss the prediction of interplanetary magnetic field (IMF) polarity (such as the north/south arrival) because we consider it too uncertain as yet for this review. Finally, in section 3, we note the new observations in Solar Cycle 24 that could be incorporated and absorbed in future prediction models. A summary and discussion will be given in section 4.

2. Current Models

Models in CME/shock arrival time prediction can be coarsely divided into the following kinds: empirical models, expansion speed model, drag-based models, physics-based models, and MHD models. It needs to be pointed out that this classification, which is based on principle and/or method of the prediction models, is only a simple arrangement of current models. It may not cover all those in this aspect.

2.1. Empirical Models

Here we define one kind of models, which adopt relatively simple equations to fit the relations between the CME disturbance's arrival time at Earth and their observables near the Sun (such as initial velocity), as empirical prediction models. The fitted equations are brief and usually analytic so that the empirical model is relatively simple and easy to use.

Vandas et al. [1996] studied the propagation and evolution of loop-like magnetic clouds in the ambient solar wind flow using ideal MHD equations. They found that the magnetic clouds and their shocks reach a nearly constant asymptotic velocity shortly after their injection. The transit time (in hours) to 1 AU for the CME flux rope's leading edge is $T_{\text{driver}} = 85–0.014\ V_i$ for a slow background solar wind speed (say, 361 km/s), and $T_{\text{driver}} = 42–0.0041\ V_i$ for a faster background solar wind speed (say, 794 km/s). Here V_i (km/s) is the propagation speed of the CME's leading edge at 18 R_s (solar radius). Then the transit time of the shock preceding the magnetic cloud is T_{shock} (h) = 74–0.015 V_i for slow solar wind and T_{shock} (h) = 43–0.006 V_i for fast solar wind.

Brueckner et al. [1998] computed the time duration of eight CMEs observed by SOHO/LASCO with the onset of geomagnetic storms during the period March 1996 through June 1997. It was found that the travel time between the explosion of CMEs on the Sun and the time when *Kp* reached its maximum value was about 80 h for 6 events. Bruecker's 80 h rule is probably the simplest one of the empirical prediction models.

One of the most typical and widely used empirical prediction models is the empirical CME arrival (ECA) and empirical shock arrival (ESA) models developed by *Gopalswamy* and his collaborators. Based on the fact that CMEs exhibit a much wider range of speeds near the Sun than the corresponding ICMEs at 1 AU, *Gopalswamy et al.* [2000, 2001] assumed that CMEs undergo an "effective" constant acceleration or

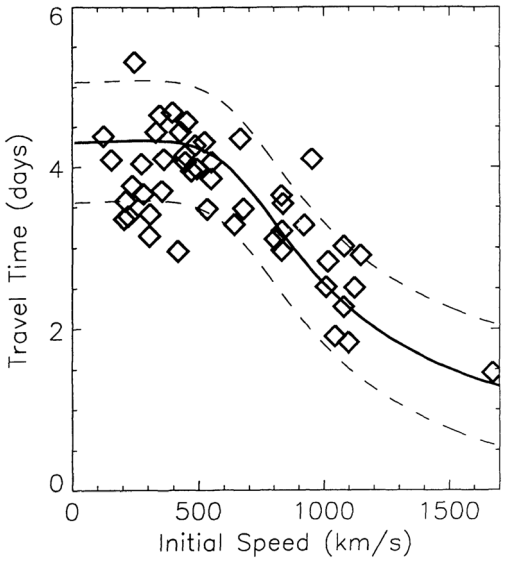

Figure 1. A representative prediction curve of the CME travel time at 1 AU for the ECA model with an acceleration cessation distance of 0.76 AU. The dashed lines are the 18 h boundaries of the prediction, and the diamonds denote the observed travel times of CMEs. Originally published in *Gopalswamy et al.* [2001].

deceleration process during their propagation outward. The acceleration or deceleration is determined by the CME's initial speed, i.e.,

$$a = \alpha - \beta u, \quad S = ut + 0.5at^2 \tag{1}$$

Here a is the effective interplanetary acceleration, u is the initial CME speed, S is the helio-distance that a CME propagates to (1 AU for the Earth) with the transit time of t. Usually, the effective acceleration will stop at a cessation distance d_1 before 1 AU, then the CME propagates at a constant speed for the remained distance $d_2 = 1\ \text{AU} - d_1$:

$$t_1 = \frac{-u + \sqrt{u^2 + 2ad_1}}{a}, \quad t_2 = \frac{d_2}{\sqrt{u^2 + 2ad_1}} \tag{2}$$

The total transit time $t = t_1 + t_2$ can be calculated from the above equations. This is the ECA model for the CME's arrival time prediction as seen in Figure 1. The ECA model had been extended by *Gopalswamy et al.* [2005] based on the gas dynamic piston-shock relationship to derive the ESA model, which provides a simple method to get the 1 AU speed and arrival times of interplanetary shocks. The primary input to both the ECA and ESA model is the initial speed (maximum in the plane-of-sky) of white-light CMEs obtained from the coronagraph observations. The ESA model has been tested using sky plane speed of CMEs from SOHO with corrections of projection effects based on Cone models by *Xie et al.* [2006] and tested using quadrature observations from STEREO by *Gopalswamy et al.* [2013].

Wang et al. [2002] found that for the CMEs that produced severe geomagnetic storms ($Kp \geq 7$), the relation between the CME-projected speeds and their transit times can be fitted by the following simple formula:

$$T_{au} = 27.98 + \frac{2.11 \times 10^4}{V} \tag{3}$$

where T_{au} (h) is the transit time and V (km/s) is the projected speed of CMEs. Similarly, *Zhang et al.* [2003] studied 26 CMEs associated with major geomagnetic storms ($Dst \leq -100$ nT) occurring between 1996 and 2000 and obtained a good correlation between CME transit time from the Sun to the near-Earth space (T, in hours) and the CME initial velocity (V, in unit of km/s) at the Sun, which can be simply described as

$$T = 96 - \frac{V}{21} \tag{4}$$

They pointed out that this formula is most accurate for fast events (e.g., $V > 500$ km/s). In a related study, from the regression analysis of 64 geoeffective CMEs that produced major geomagnetic storms ($Dst < -100$ nT) during 1996–2002, *Srivastava and Venkatakrishnan* [2004] derived the following relation between the transit time (in hours) of CMEs and their initial speed (in km/s):

$$T = 86.9 - 0.026\ V \tag{5}$$

Manoharan et al. [2004], using IPS, investigated 91 interplanetary shocks associated with CMEs originating within about ±30° in heliographic longitude from the center of the Sun during 1997–2002. They compared the shocks' speed and transit time at 1 AU and noted that the shock transit time is not controlled by its final speed but is primarily determined by the initial speed of the CME and effects encountered by it during the propagation in interplanetary space. The best fit curve to the transit times of all shocks versus the initial speeds of the associated CMEs is the following:

$$t_{\text{shock}} = 3.9 - 2 \times 10^{-3}\ V_{\text{CME}} + 3.6 \times 10^{-7}\ V_{\text{CME}}^2 \tag{6}$$

Here t_{shock} is the shock's transit time in unit of days determined as the interval from the first appearance of the associated CME in the FOV of LASCO/C2 to the interplanetary shock's arrival at WIND. V_{CME} is the initial speed of the CME obtained from a linear fit to the "height-time" measurements of SOHO/LASCO in the plane-of-sky.

Based on the observation of (1) the white-light images of SOHO/LASCO in the near-Sun region and (2) the interplanetary scintillation (IPS) images of the inner heliosphere obtained from the Ooty Radio Telescope, the radial evolution from the Sun to the Earth of 30 wide CMEs (angular width >150°) has been investigated by *Manoharan* [2006]. The following quadratic polynomial equation is derived to best fit the data points between CME's transit time (T_{CME}, in hours) and its initial speed (V_{CME}, in km/s):

$$T_{CME} = 108.6 - 0.5 \times 10^{-1}\ V_{CME} + 1.1 \times 10^{-5}\ V_{CME}^2 \tag{7}$$

According to this equation, it takes a CME with the speed of 400 km/s about 90 h to propagate from the Sun to the Earth's orbit. But it takes solar wind moving constantly at this speed about 103 h to finish the 1 AU distance. *Manoharan* [2006] suggested that the difference of 13 h in transit times reveals that the propagation of the CME is supported by its stored internal energy.

Utilizing 91 CME-IP (interplanetary) shock events during the period 1997 to 2002, *Kim et al.* [2007] evaluated the performance of the ESA model. They pointed out that the prediction error was within ±12 h for 60% (55 events) of the total events. The deviations of shock arrival times from the ESA model during solar maximum were correlated with the CME initial speeds (V_{CME}), which indicates that the constant interplanetary acceleration in the ESA model does not apply well for all CME events. They derived a linear fit to the relationship between shock's transit time T (in hours) and V_{CME} (in km/s) during solar maximum after the linear regression analysis:

$$T = 76.86 - 0.02\ V_{CME} \tag{8}$$

Vršnak and Žic [2007] analyzed the relationship between CME's transit time (T), CME speed (v_{CME}), and the background solar wind speed (w) based on two samples of CME-ICME events. One is the S-sample compiled by *Schwenn et al.* [2005]; the other is the H-sample complied by *Howard and Tappin* [2005]. It was found that CME transit times depend on both the CME take-off speed and the background solar wind speed. The transit times of CMEs that are associated with solar wind faster than 500 km/s are shorter by 20–30 h than those associated with the wind slower than 400 km/s on average. They performed a two-parameter linear least squares fit concerning the CME's transit time, which is

$$V_T = k_0 + k_1 v_{CME} + k_2 w \tag{9}$$

Here V_T is the transit speed of the CME defined as the ratio of the distance traveled by ICME and the corresponding transit time T; the correlation parameters for S-sample are $k_0 = -111 \pm 75$ km/s, $k_1 = 0.16 \pm 0.03$, and $k_2 = 1.41 \pm 0.18$. The other symbols (V_T, v_{CME}, and w) are in units of km/s.

Based on the constraints imposed by the Type II low-frequency decametric/kilometric radio emissions generated by shocks driven by CMEs, the measured 1 AU transit times and the calculated in situ shock speeds, together with the required consistency with the white-light measurements, *Reiner et al.* [2007] presented a comprehensive study of the interplanetary transport of 42 CME/shocks during Solar Cycle 23. They found that the 1 AU transit time correlates well with neither the initial CME speed nor its deceleration. The distance and time over which a CME decelerates depends on its initial speed and the conditions of the interplanetary medium, which are greatly different from one CME to another. The stopping distance of the CME's deceleration ranges from 0.2 to beyond 1 AU. The faster CME/shocks tend to decelerate more rapidly near the Sun within shorter time periods. Their conclusions would be useful for developing arrival time prediction algorithms.

During the SOHO era, the CME initial speed is obtained from the white light observations of coronagraph (SOHO/LASCO), which will undergo inevitable projection effects. The CME speed derived in this way, as noted earlier, is the projected speed on the plane-of-sky. The radial speeds of CMEs, especially their speeds in the Earth's direction are crucial for predicting the arrival times of CMEs at Earth. *Michalek et al.* [2008] defined an asymmetry ratio (ASR) as the ratio between the maximum and minimum projected speed, i.e., $ASR = <V_{max}> / <V_{min}>$. Then they put forward a new way to estimate the space speed of CMEs, which is $V_{imp} = <V_{max}> + <V_{max}>/ASR$. They applied this technique to "halo CMEs" (i.e., CMEs apparently

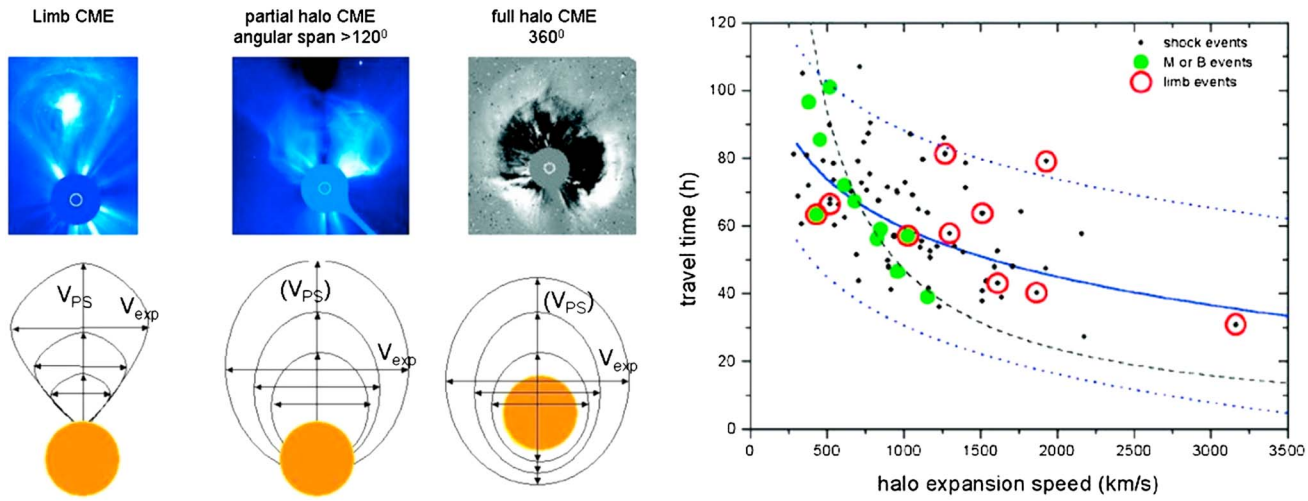

Figure 2. (left) The definition of CME expansion speed and (right) the CME travel time to 1 AU plotted versus its expansion speed. Originally published in *Schwenn et al.* [2005].

propagating along the Sun-Earth line) observed during 2001–2002 and obtained that the improved speeds correlated better with the transit times of halo CMEs at Earth.

2.2. Expansion Speed Model

Considering the fact that the radial propagation speed of halo CMEs could not be measured directly during the SOHO era (as viewed by a single spacecraft's coronagraph), *Schwenn et al.* [2005] pointed out that the radial speed of CME correlates well with its lateral expansion speed (V_{exp}) after inspecting 57 representative limb CMEs observed by SOHO/LASCO. Therefore, the lateral expansion speed may serve as a proxy for the inaccessible radial speed of halo CMEs. On this basis, they obtained the following formula fitting the data best to predict the arrival time of CMEs at Earth:

$$T_{tr} = 203 - 20.77 \times \ln\left(V_{exp}\right) \tag{10}$$

where T_{tr} (in hours) is defined between the CME's first appearance in LASCO/C2 images and the CME-associated shock's arrival at 1 AU, V_{exp} (in km/s) is the expansion speed of halo CMEs near the Sun. The prediction of this formula for 75 CME-shock events demonstrates that there is a 95% probability that the shock will arrive within 1 day around that predicted time unless it is one of the 15% of CMEs that never hit the Earth. The definition of V_{exp} and the variation of CME travel time plotted against V_{exp} can be found in Figure 2.

2.3. Drag-Based Models

Many observations reveal that faster CMEs undergo decelerations in interplanetary space while slower CMEs undergo accelerations, which demonstrates a tendency of CMEs to adjust speed toward the background solar wind. In other words, the dynamics of CMEs are governed mainly by their interaction with the background solar wind beyond a certain helio-distance. Based on these foundations, a class of analytical models has been developed to depict the propagation of CMEs and predict their arrival times. This kind of model is based on the motion equation of CMEs where the drag acceleration/deceleration has a quadratic dependence on the relative speed between CMEs and the background solar wind. Therefore, they are called "drag-based models" in this paper.

Vršnak [2001] studied the deceleration of 12 coronal eruptions. It was found that the measured deceleration rates depend on the events' plane-of-sky velocities and heights, and this dependence on the velocity can be described better by a quadratic function than by linear fit. In order to interpret this phenomenon, a viscous drag (following classical aerodynamic empiricism) was introduced into the motion

of CMEs. After considering the force acting on a segment of the flux rope, the acceleration of the magnetic flux rope eruption can be modeled as

$$\dot{v} = f_L - g - f_{\text{visc}} \tag{11}$$

where f_L, g, and f_{visc} stand for the Lorentz force, gravity, and viscous drag term, respectively. Appropriate expressions for the viscous drag are either a linear term or a quadratic term of the velocity as demonstrated by numerical MHD simulations [*Cargill et al.*, 1996]:

$$f_{\text{visc}} = \gamma_1 (v - w) \tag{12}$$

$$f_{\text{visc}} = \gamma_2 |v - w| (v - w) \tag{13}$$

Here v is the CME speed, w is the solar wind speed, γ_1 and γ_2 are coefficients that depend on the density and viscosity of the ambient plasma as well as on the geometrical proportions of the CME body. The radius of the flux rope and the density ratio change with the helio-distance, and the dependences on distance of γ_1 and γ_2 could not be obtained in an explicit form. *Vršnak and Gopalswamy* [2002] adopted the empirical expressions of the parameters γ_1 and γ_2 with the heliocentric distance, R (R_s), as $\gamma_{1,2} = \alpha_{1,2} R^{-\beta_{1,2}}$, where α and β are constants determined empirically. Then the motion equation of CMEs could be rewritten into the following forms after neglecting the Lorentz force and the gravity in late phases of CME eruption:

$$\frac{\mathrm{d}v}{\mathrm{d}R} = R_s \alpha_1 R^{-\beta_1} \left(1 - \frac{w}{v}\right) \tag{14}$$

$$\frac{\mathrm{d}v}{\mathrm{d}R} = R_s \alpha_2 R^{-\beta_2} \left(1 - \frac{w}{v}\right) |v - w| \tag{15}$$

In order to predict the arrival time of the CME, the variation of w along distance R is needed, which is provided by the solar wind model of *Sheeley et al.* [1997]:

$$w(R) = w_0 \sqrt{1 - e^{-(R - R_b)/R_a}} \tag{16}$$

where $w_0 = 298.3$ km/s, $R_b = 2.8$, and $R_a = 8.1$. Equations (14) and (15) were integrated numerically by *Vršnak and Gopalswamy* [2002] together with equation (16) to determine the model transit times ($T_{1\ \text{AU}}$) and velocities ($v_{1\ \text{AU}}$) of CMEs at 1 AU as a function of the initial velocity v_0. The results reproduce well the observations in the statistical sense. This analysis has been extended by *Shanmugaraju and Vršnak* [2014] to derive in more detail the dependence of the CME's transit time on its speed and the background solar wind speed for different combinations of α and β.

Cargill [2004] discussed the aerodynamic drag force experienced by CMEs through numerical simulations. It was found that the drag force is proportional to the square of the relative speed between CMEs and the background solar wind as well as a dimensionless drag coefficient (C_D). The drag coefficient depends on the relative density of CMEs with respect to the solar wind. The drag coefficient increases from unity to much greater value if the CME's relative density decreases from dense to tenuous. Although the drag coefficient remains to be a constant during the majority of the CME journey from the Sun to 1 AU, an evident radial dependence of C_D exists for the extremely tenuous CMEs. These results help us to further understand the aerodynamic drag effects in the propagation of CMEs. *Vršnak et al.* [2010] studied solutions of these drag-based equations by systematically varying the input parameters. It was found that the speeds of wide CMEs of low masses approach the solar wind speed quickly near the Sun; therefore, their transit times are mainly determined by the background solar wind speed. Narrow and massive CMEs moving in the fast solar wind streams would reach the Earth with short transit time and fast propagating speed at 1 AU.

Song [2010] simplified equation (13) with the assumption that the coefficient γ_2 is a constant, and in this way got the following formula to describe the motion of CMEs:

$$\dot{v} = -\frac{1}{A}(v - w)^2 \tag{17}$$

The integral of this equation yields the following:

$$\frac{\Delta T}{A} = \frac{1}{V_{\text{ICME}} - V_{\text{SW}}} - \frac{1}{V_{\text{CME}} - V_{\text{SW}}} \tag{18}$$

$$L = V_{\text{SW}} \Delta T + A \ln \frac{V_{\text{CME}} - V_{\text{SW}}}{V_{\text{ICME}} - V_{\text{SW}}} \tag{19}$$

where A and L are constants. For the four parameters V_{CME}, V_{ICME}, ΔT, and V_{SW}, Equations (18) and (19) could be solved to give the prediction of V_{ICME} and ΔT if V_{CME} and V_{SW} are input. In real applications, V_{CME} can be obtained from the observation of SOHO/LASCO. The limitation of this model is the difficulty in determining V_{SW}, which can be supplied by interplanetary observations or predicted by solar wind numerical computational methods.

Subramanian et al. [2012] discussed the variation of the drag coefficient (C_D) by adopting a microphysical prescription for viscosity in the turbulent solar wind to obtain an analytical model for the drag coefficient. The equation that they advocated is the following:

$$m_{CME}V_{CME}\frac{dV_{CME}}{dR} = \frac{1}{2}C_D N_i m_p A_{CME}(V_{CME} - V_{SW})^2 \tag{20}$$

Here N_i is the proton number density, m_p is the proton mass, and A_{CME} is the cross-sectional area of the CME. It is believed that the drag coefficient C_D is determined from the sonic Mach number (M_s) or Reynolds number (Re) of the system, which are determined from the CME velocity V_{CME}, the typical macroscopic length scale R_{CME} and the viscosity coefficient. Their work is the first physical characterization of the aerodynamic drag experienced by CMEs (considered as solid objects that cannot be valid). Their derived velocity profiles, nevertheless, agree well with observations of deceleration experienced by fast CMEs.

Vršnak et al. [2013] simplified the drag-based model and presented an explicit solution for the Sun-Earth transit time of CMEs and their impact speed at 1 AU. The start equation is the quadratic form for the drag acceleration:

$$\frac{d^2r}{dt^2} = -\gamma(r)\left(\frac{dr}{dt} - w(r)\right)\left|\frac{dr}{dt} - w(r)\right| \tag{21}$$

where r is the helio-distance of the CME's leading edge and $w(r)$ is the background solar wind speed. For the simplest case when $\gamma(r)$ = constant and $w(r)$ = constant, the analytical solutions of equation (21) give

$$v(t) = \frac{v_0 - w}{1 \pm \gamma(v_0 - w)t} + w \tag{22}$$

and

$$r(t) = \pm\frac{1}{\gamma}\ln[1 \pm \gamma(v_0 - w)t] + wt + r_0 \tag{23}$$

where the sign of $\pm$ is positive for $v_0 > w$, and negative for $v_0 < w$; v_0 is the CME "take-off speed" at r_0. In this way, the simplest version of drag-based models (DBM) provides the explicit solution of $r(t)$, $v(t)$, and $v(r)$ relation. The transit time of a CME and its "impact speed" to any helio-distance r can be obtained analytically with the input of v_0, r_0, and the ambient solar wind speed w. The differences between this simplest DBM model to those of $\gamma(r) \neq$ constant and $w(r) \neq$ constant are discussed and found to be very small beyond 20 R_s. Figure 3 shows examples of the CME's kinematics based on this DBM model. In real applications, r_0 and v_0 can be obtained from the coronagraph observations of CMEs, w is taken either as a constant within the range of 300–600 km/s or from the in situ measurements of spacecraft, and γ is taken to be a constant within the range of $2\times10^{-8} - 2\times10^{-7}$ km^{-1}. The value ofγ is taken close to the lower limit of 10^{-8} km^{-1} for high density CMEs, while it is taken near the upper limit of 10^{-7} km^{-1} for low-density CMEs. Especially, a public online forecast tool has been developed based on this DBM (http://oh.geof.unizg.hr/DBM/dbm.php), which enables the easy handling and straightforward application of this model to real-time space weather forecasting.

2.4. Physics-Based Models

In contrast to the empirical prediction models that use simple equations from fitting observations to give the arrival time prediction, the physics-based prediction models are often based on certain physics theory or concept. They use the observed CME-IP disturbance events as samples to "train" the theoretical model and give predictions in real applications.

The "Shock Time of Arrival" (STOA) model is based on similarity theory of blast waves from point explosions revised by the piston-driven concept [*Dryer*, 1974; *Dryer and Smart*, 1984; *Smart and Shea*, 1984, 1985]. According to STOA, the initial explosion produces a shock, which propagates at a constant speed (V_{si}) for a piston-driving time duration (τ) and then decelerates to a blast wave with $V_s \sim R^{-1/2}$ (R is the heliocentric radial distance). A cosine function is adopted to consider the longitudinal dependence of the shock's geometry in

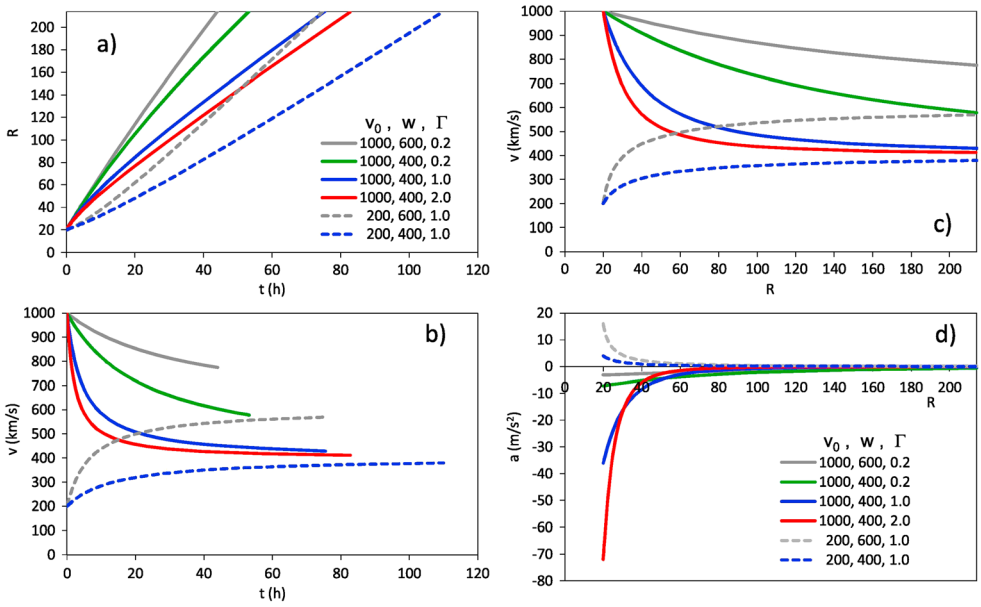

Figure 3. Examples of the CME kinematics based on DBM with $r_0 = 20\ R_s$. (a) CME leading edge distance against time, (b) CME speed against time, (c) CME speed against distance, and (d) CME acceleration against distance. Here v_0 and w are in unit of km/s, $\Gamma = \gamma \times 10^7$ km^{-1}. Originally published in *Vršnak et al.* [2013].

the ecliptic plane, and the shock speed is assumed to decrease from maximum in the direction of the flare via this cosine function to provide a nonspherical shape in longitude. The initial shock speed is calculated from United States Air Force/Australian ground-based Type II metric radio frequency drift rate based on an assumed coronal density model. STOA considers a variable background solar wind speed through which the shock propagates, and this solar wind speed (V_{sw}) is estimated from in situ measurements of solar wind at L1 spacecraft at the time of the flare. The input parameters of STOA are as follows: the solar flare longitude, the start time of metric Type II radio burst, the initial shock speed, the proxy piston-driving time duration, and the background solar wind speed. The outputs of STOA include the arrival time of the shock at any radial distance in the ecliptic plane as well as whether the shock will arrive at this position by adoption of the shock's Alfvén Mach number (*Ma*) as an indicator of the expected shock strength.

Moon et al. [2002] examined the possibility for improvement of the STOA model concerning the radial variation of shock velocity. They pointed out that the radial dependence of shock wave velocity depends on its initial velocity as demonstrated by observational and numerical findings. Therefore, they suggested a simple modified STOA-2 model, which has a linear relationship between initial coronal shock wave velocity (V_{is}) and its deceleration exponent (N), i.e., $N = 0.05 + 4 \times 10^{-4}\ V_{is}$. Both the input and output of STOA-2 are the same as those of STOA. Their results reveal that the STOA-2 model could remove the systematic dependence of the prediction error of the original STOA model on the initial shock velocity.

The "Interplanetary Shock Propagation Model" (ISPM) is based on a 2.5-D MHD parametric study of numerically simulated shocks, which demonstrates that the organizing parameter for the shock is the net energy released into the solar wind [*Smith and Dryer*, 1990, 1995]. The transit time of the shock and its strength at 1 AU is given by algebraic equations in the model in terms of the net energy released by a solar event into the solar wind and its source's longitude. As the energy released by a solar event is not a parameter measured directly, ISPM provides an empirical method to estimate the net input energy from proxy solar data. The inputs of ISPM are the same as those of STOA except for the background solar wind speed V_{sw}, which is chosen to be a heliolongitudinally fixed radial profile with $V_{sw} = 340$ km/s at 1 AU. Thus, corotating stream-stream nonuniform interactions are not considered. Besides the shock's transit time at 1 AU, ISPM also outputs the shock strength index (SSI), which is computed from the logarithm (base 10) of the normalized dynamic pressure jump, as an indicator to predict whether the shock would reach the desired location (such as the Earth).

The "Hakamada-Akasofu-Fry version 2" (HAFv.2) model is a "modified kinematic" solar wind model that calculates the solar wind speed, density, magnetic field, and dynamic pressure as a function of time and

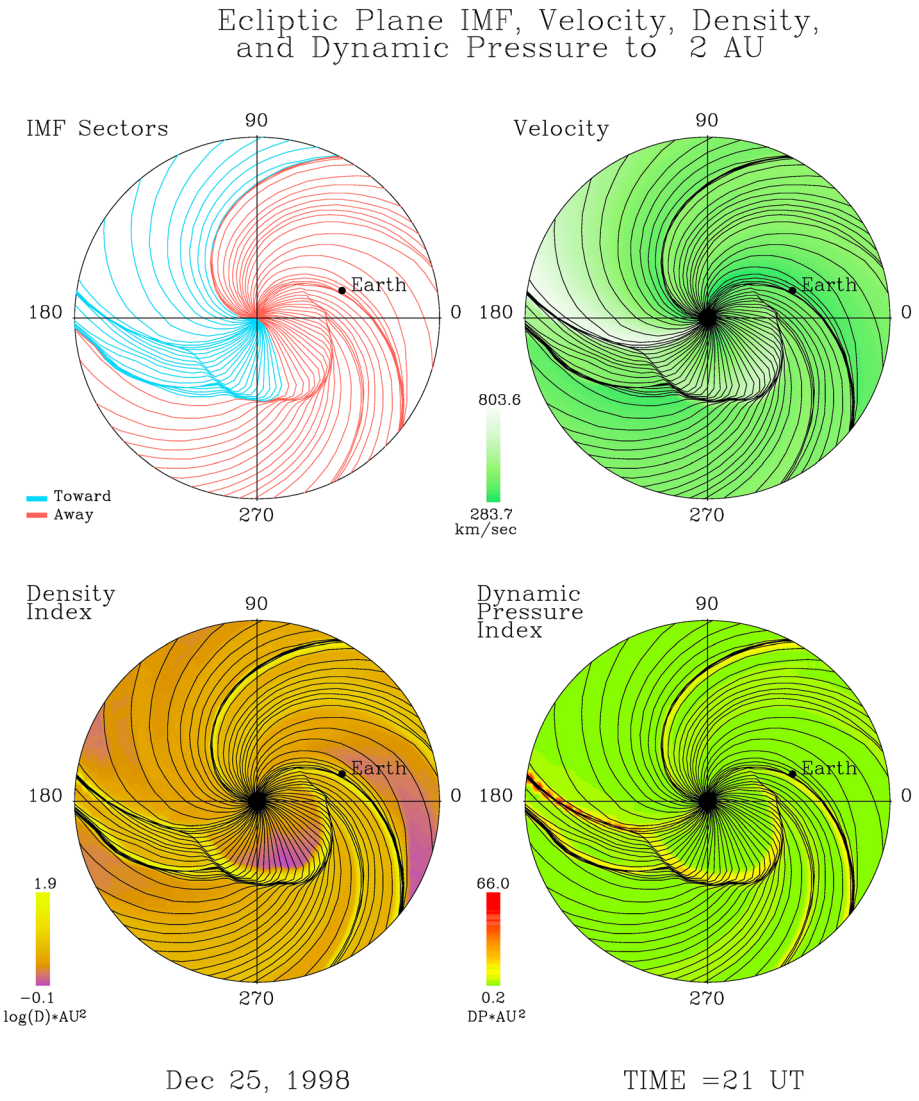

Figure 4. Solar wind conditions to 2 AU in the ecliptic plane predicted by HAFv.2 for the 23 December 1998 flare/Type II-shock event. (top left) Interplanetary magnetic field (IMF) pattern, (top right) solar wind velocity, (bottom left) proton density with IMF pattern, and (bottom right) predicted dynamic pressure. Originally published in *Fry et al.* [2003].

location [*Dryer et al.*, 2001, 2004; *Fry et al.*, 2001, 2003, 2007; *McKenna-Lawlor et al.*, 2002, 2006, 2012; *Smith et al.*, 2005, 2009a; *Sun et al.*, 2002, 2003]. This model gives a global description of the propagation of multiple and interacting shocks in nonuniform, stream-stream interacting flows of solar wind in the ecliptic plane. In contrast to MHD simulations, the HAFv.2 model begins with the equations integrated twice to give the fluid parcel positions, and velocity is derived from d*x*/d*t*. The input parameters of HAFv.2 include the input of disturbance and the input of background solar wind; the former are the same as those of STOA; while for the latter, HAFv.2 computes the ambient solar wind speed continually through the prediction method by *Arge and Pizzo* [2000] with the radial magnetic field at the source surface ($R = 2.5\ R_s$) as input. That is, realistic inner boundary conditions determine the background solar wind flow and IMF topology in the model. As for output, HAFv.2 predicts the solar wind speed, density, dynamic pressure, and IMF vector at any point in the heliosphere as a function of time. A Shock Searching Index (SSI_H) is computed at L1. When this index exceeds an empirical threshold value, a shock arrival is predicted at that time, otherwise "no shock arrival" predicted. Figure 4 gives an example of the solar wind conditions to 2 AU in the ecliptic plane predicted by HAFv.2 for the solar disturbance-IP shock event on 23 December 1998. *Smith et al.* [2009b] examined the model verification and performance of HAFv.2 as a function of input parameters, and found that it was possible to categorize the prediction outcomes by defining three thresholds for the input speed, duration, and X-ray class.

The STOA, ISPM, and HAFv.2 models use similar input solar parameters (i.e., the source location of the associated flare, the start time of the metric Type II radio burst, the proxy piston driving time duration, and the background solar wind speed) and predict not only the shock arrival times but also whether or not the interplanetary shock can encounter the Earth by introducing a judgment index (i.e., *Ma* in STOA, SSI in ISPM, and SSI_H in HAFv.2). They have been used to give the "near real-time" predictions for the arrival of interplanetary shocks at Earth using solar data available to forecasters as inputs since February 1997. An event list of more than 600 solar disturbance-IP shock events has been built up during the time period February 1997 to December 2006 covering nearly the entire Solar Cycle 23. Their rigorous statistically based predictions are frequently referred to in the literature as "Fearless Forecasts," and the prediction results were sent to interested members of both scientific and operational communities through emails within 10 h after the solar events. The performances of the above three models have been tested and the comparative study revealed that the performances of these three models are very similar in real-time forecasting of the shock's arrival at Earth. Details about the predictions of the Fearless Forecast models and the information for their database events can be found at the website http://www2.gi.alaska.edu/pipermail/gse-ff/.

There are other physical models established on the basis of the Fearless Forecast models. A practical database method for predicting the interplanetary shock arrival time at L1 point was presented by *Feng et al.* [2009] based on the predicting performance of the HAF model to a set of "hypothetical solar events" and an empirical correction to its prediction results. They first established a shock transit time Database-I based on HAFv.1 with hypothetical solar events. Then, they modified Database-I to create a practical Database-II via the prediction test for the real observed solar events, which was organized on a multidimensional grid of source location, initial coronal shock speed, and the year of occurrence of the hypothetical solar event. The arrival time at L1 for any given solar event occurring in Solar Cycle 23 could be predicted by looking up in the grid of Database-II according to source location, the initial coronal shock speed, and the year of occurrence.

By considering the detection of energetic particles at L1, *Qin et al.* [2009] created two new models, STSEP and STOASEP, based on STOA. They added the use of solar energetic particles (SEPs) detected at Earth to improve the shock arrival time prediction of the STOA model. It demonstrates that the shock arrival prediction is improved by the new models with the help of 38–53 keV electron SEP observations. In particular, the ratio of the correct prediction to false alarm becomes greatly enhanced.

Liu and Qin [2012] combined the soft X-ray observations at L1 with the STOA model in predicting the shock arrival time and obtained two other methods, i.e., STOAF and STOASF. Testing the methods with 585 solar flare-type II burst events during the period September 1997 to December 2006, it is found that the two new methods get higher success rate, which demonstrates the possibility of using the soft X-ray data to improve the shock arrival time prediction.

Interplanetary shocks, especially those with strong geomagnetic effects, often accelerate energetic ions during their propagation. These energetic ions are useful to monitor the progress toward the Earth of the interplanetary shocks and provide "fine-tuning" of predictions made on the basis of solar observations. Therefore, the observation of energetic ion enhancements at satellites located at L1 is a potential tool for predicting the arrival of interplanetary shocks hours before they arrive at L1 [*Smith et al.*, 2004]. *Smith and Murtagh* [2009] presented a forecast tool for predicting large geomagnetic storms ($Kp \geq 7$) following the arrival of interplanetary shocks at 1 AU based on the observations of low-energy energetic ions (47–65 keV) and solar wind data at the L1 point. This model has been (still ongoing) tested by the Australian Space Forecast Centre (http://www.ips.gov.au/mailman/listinfo/ips-swp-alert). *Aran et al.* [2006] developed SOLPENCO (Solar Particle Engineering Code) as the first step toward an operational tool able to quantitatively predict proton flux and fluence profiles of SEP events associated with interplanetary shocks. SOLPENCO can also provide an estimate for the transit time and average speed of the CME-driven shock (http://dev.sepem.oma.be/help/solpenco2_intro.html).

Combining the analytical study for the propagation of the blast wave from a point source in a moving, steady state, medium with variable density [*Wei*, 1982; *Wei and Dryer*, 1991] with the energy estimation method in the ISPM model [*Smith and Dryer*, 1990, 1995], *Feng and Zhao* [2006] presented a new "Shock Propagation

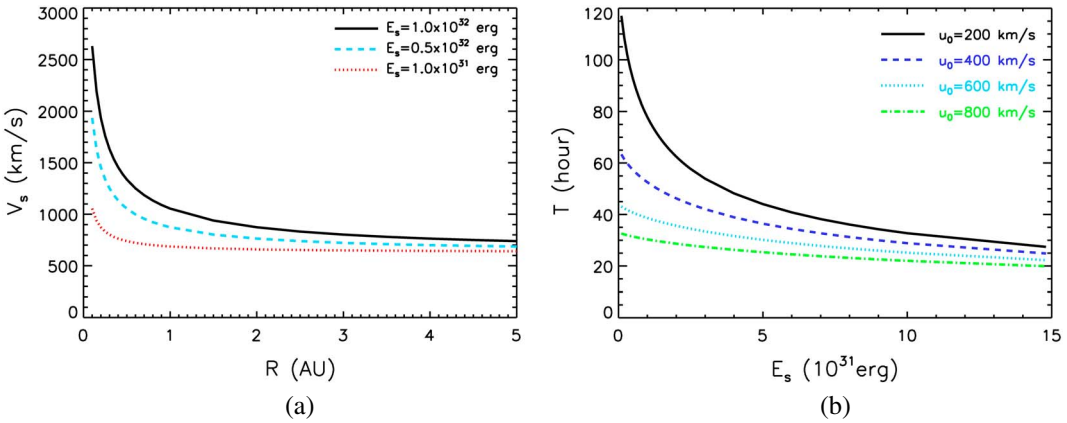

Figure 5. (a) The shock propagating speed versus distance for different energies (E_s) with fixed solar wind speed $u_0 = 400$ km/s predicted by SPM and (b) the shock's transit time to 1 AU versus the shock energy for different u_0 by SPM. Figure 5b is adapted from *Feng and Zhao* [2006] with redrawing.

Model" (SPM) to predict the arrival time of interplanetary shocks at Earth. They started from the basic equations of ideal fluid dynamics with a spherically symmetric hypothesis:

$$\begin{aligned} \frac{\partial \rho}{\partial t} + u\frac{\partial \rho}{\partial r} + \rho\left(\frac{\partial u}{\partial r} + \frac{2u}{r}\right) &= 0 \\ \rho\left(\frac{\partial u}{\partial t} + u\frac{\partial u}{\partial r}\right) + \frac{\partial p}{\partial r} &= 0 \\ \frac{\partial p}{\partial t} + u\frac{\partial p}{\partial r} + \gamma p\left(\frac{\partial u}{\partial r} + \frac{2u}{r}\right) &= 0 \end{aligned} \tag{24}$$

A series of dimensionless variables are defined to solve the equations after modifying Sedov's classical similarity theory for the blast waves to include a steady state, background solar wind flow. After several steps of complicated deductions and reasonable simplifications, the following equation is obtained to depict the variation of the shock's speed (V_s) with the distance of the shock front (R) from the Sun:

$$V_s = \frac{dR}{dt} = \left[-2\lambda_1 + \sqrt{(2\lambda_1)^2 + \frac{E_0}{J_0 R} + \frac{1}{2J_0}}\right] u_0 \tag{25}$$

Here u_0 is the background solar wind velocity, E_0 represents the dimensionless form of the total energy E_s, $E_0 = E_s/Au_0^2$, $J_0 = 3/8$, $\lambda_1 = -0.1808$, and $A = 300$ kg/m. Figure 5a gives the helio-distance variation of the shock's propagation speed for different energies of the associated solar blast with fixed $u_0 = 400$ km/s based on equation (25). The integral of equation (25) gives the transit time (T) of the shock to reach a position R:

$$\begin{aligned} T = \int \frac{dR}{V_s} = \frac{J_0}{u_0}\Bigg\{ & 4\lambda_1[R + 2E_0 - 2E_0 \ln(R + 2E_0)] + 2\sqrt{X} - \frac{\left(16\lambda_1^2 + \frac{1}{J_0}\right)E_0}{\sqrt{4\lambda_1^2 + \frac{1}{2J_0}}} \\ & \times \ln\left[\sqrt{X} + (R + 2E_0)\sqrt{4\lambda_1^2 + \frac{1}{2J_0}} - \frac{\left(16\lambda_1^2 + \frac{1}{J_0}\right)E_0}{2\sqrt{4\lambda_1^2 + \frac{1}{2J_0}}}\right] \\ & - 8\lambda_1 E_0 \times ln\left[\frac{\sqrt{X} + 4\lambda_1 E_0}{R + 2E_0} - \frac{16\lambda_1^2 + \frac{1}{J_0}}{8\lambda_1}\right]\Bigg\} + T_0 \end{aligned} \tag{26}$$

where $\sqrt{X} = \sqrt{\frac{E_0}{J_0}R + \left(4\lambda_1^2 + \frac{1}{2J_0}\right)R^2}$, T_0 is determined by the restriction of $R = 0$ when $T = 0$. If the total energy of a solar blast and the background solar wind speed are known, then the arrival time of the corresponding

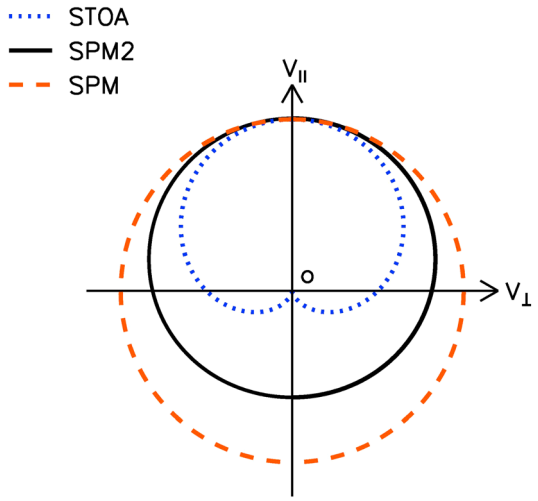

Figure 6. Comparison of the shock front speed profile for STOA (dotted blue line), SPM (dashed red line), and SPM2 (solid black line). $V_{\parallel}$ and $V_{\perp}$ represent the shock speed in the directions parallel and perpendicular to the maximum propagation direction. Originally published in *Zhao and Feng* [2014].

shock to any radial distance can be computed from equation (26). Similarly, Figure 5b demonstrates the transit time of the shock to 1 AU plotted versus the total energy for different ambient solar wind speeds according to equation (26). The total energy of a solar blast, however, is not a parameter readily available from direct observations. Fortunately, ISPM provides a simple method to estimate the energy of a solar event, which assumes that the total energy of the event is proportional to its kinetic energy flux $\left(V_s^3\right)$, the longitudinal width (ω), and the duration of the initial pulse (τ):

$$E_s = CV_s^3\omega(\tau + D) \tag{27}$$

Here $C = 0.283 \times 10^{20}$ erg m^{-3} s^{-2} deg^{-1}, $D = 0.52$ h, and an average of angular width $\overline{\omega} = 60°$ are adopted in ISPM. Equations (26) and (27) constitute the SPM model. The inputs of SPM include the duration of the X-ray flare, the initial shock speed, and the background solar wind speed. The output of SPM gives the predicted transit time of the shock to any radial distance R. Applying SPM to 165 solar events during the periods of January 1979 to October 1989 and February 1997 to August 2002, it is found that the relative error is ≤ 10% for 27.88% of all events, ≤ 30% for 71.52%, and ≤ 50% for 85.46%. This study demonstrates a potential capability of SPM in terms of real-time forecasting.

However, the SPM model presently requires upgrading as follows. (1) It predicts only arrival times of interplanetary shocks and cannot predict whether or not an interplanetary shock would arrive at Earth as the Fearless Forecast models. (2) The blast wave theory may not be suitable for all the shocks. *Li et al.* [2008] pointed out that the propagation of some shocks deviates much from the prediction limit of SPM. (3) According to the blast wave theory adopted in SPM, the shock propagates outward with a circular front so that the arrival time predicted by SPM has no dependence on its propagating direction, which neglects the contribution of shock's propagation direction on its arrival time. (4) The initial speed of the shock wave, determined by metric Type II radio burst, is used to estimate the energy of the shock; due to the lack of spatial information of the radio bursts, the shock speed derived in this way often contains some uncertainties. All these issues constitute hindrances for the prediction precision of SPM. In order to lessen these drawbacks and promote the prediction capability of SPM, *Zhao and Feng* [2014] put forward its updated version, i.e., SPM2. Considering the corrections in the above indicated steps, SPM2 uses the following equation to compute the propagation speed of the shock at the Earth's location (V_s (EL)):

$$V_s = \frac{dR}{dt} = \left[-2\lambda_1 + \sqrt{(2\lambda_1)^2 + \frac{E_0}{J_0 R} + \frac{1}{2J_0}}\right] u_0 \times F_{AD} \times F_{PD} \tag{28}$$

Here F_{AD} and F_{PD} denote the acceleration/deceleration term and the propagation direction term, respectively, i.e., $F_{AD} = 1.244 - 6.28 \times 10^{-4} u_0$, $F_{PD} = 0.85 + 0.2\cos\theta\cos\varphi$, θ and φ denote the heliographic latitude and longitude, respectively, for the solar source of the associated shock; $E_0 = \frac{C\, V_{si}^{*3}\, \omega\, (\tau + D)}{A\, u_0^2}$, $V_{si}^* = \left(0.3818 - 3.0 \times 10^{-4} V_{si} \sin\theta\right) V_{si} + V_{si}$, V_{si} is the shock's initial speed computed from the type II radio burst drifting speed, $A = 300$ kg m^{-1}, $C = 0.283 \times 10^{20}$ erg m^{-3} s^{-2} deg^{-1}, $D = 0.52$ h, and $R = 1$ AU for the Earth's location. The consideration of the shock's propagation direction in its arrival time prediction mitigates the isotropy limitation of blast wave theory in real applications and results in a simplified shock front speed profile in three dimensions. Figure 6 displays the ecliptic plane projection of the shock front speed profile adopted by SPM2 (solid black line). The shock front speed profile adopted by STOA (dotted blue line) and SPM

Table 1. Statistical Comparison of the Values of a Range of Standard Forecast Skill Scores Derived by SPM2 With Those of HAFv.2, STOA, and ISPM Based on the Same Events of Solar Cycle 23 (February 1997 to December 2006)[a]

Forecast Skill Scores	Ideal Value	SPM2	HAFv.2	SPM2	STOA	SPM2	ISPM
PODy	1	0.61	0.76	0.64	0.80	0.64	0.51
PODn	1	0.61	0.41	0.62	0.37	0.61	0.63
FAR	0	0.53	0.57	0.52	0.52	0.52	0.56
BIAS	1	1.29	1.79	1.31	1.91	1.32	1.16
CSI	1	0.36	0.38	0.38	0.38	0.38	0.31
TSS	1	0.22	0.17	0.25	0.17	0.25	0.15
HSS	1	0.20	0.15	0.24	0.14	0.24	0.14
GSS	1	0.11	0.08	0.13	0.08	0.13	0.08
SR	1	0.61	0.54	0.62	0.53	0.62	0.59
X^2	N[b]	24.0	16.2	27.4	14.1	24.4	8.3
p3	0	9.5×10^{-7}	5.6×10^{-5}	1.7×10^{-7}	1.8×10^{-4}	7.8×10^{-7}	0.0039

[a]Adapted from *Zhao and Feng* [2014] with redrawing.
[b]The event number of the same data sets with SPM2, which is 551 for HAFv.2, 463 for STOA, and 418 for ISPM.

(dashed red line) are also shown in this figure. After knowing the shock's propagation speed at the Earth, an "equivalent shock strength index" of each shock is computed as

$$\mathrm{ESSI} = \frac{V_s(\mathrm{EL}) - u_0}{V_f} \tag{29}$$

where $V_f = 100$ km/s. If $\mathrm{ESSI} \geq \mathrm{ESSI_{tv}} = 2.29$, the shock is predicted to reach the Earth, while if $\mathrm{ESSI} < \mathrm{ESSI_{tv}} = 2.29$, the shock is predicted to miss the Earth. For the former case, the shock's transit time to the Earth is computed according to the following:

$$\begin{aligned} T = \frac{J_0}{\mathrm{u}_0 \times F_{\mathrm{AD}} \times F_{\mathrm{PD}}} \Bigg\{ & 4\lambda_1 [R + 2E_0 - 2E_0 \ln(R + 2E_0)] + 2\sqrt{X} - \frac{\left(16\lambda_1^2 + \frac{1}{J_0}\right) E_0}{\sqrt{4\lambda_1^2 + \frac{1}{2J_0}}} \\ & \times \ln \left[\sqrt{X} + (R + 2E_0) \sqrt{4\lambda_1^2 + \frac{1}{2J_0}} - \frac{\left(16\lambda_1^2 + \frac{1}{J_0}\right) E_0}{2\sqrt{4\lambda_1^2 + \frac{1}{2J_0}}} \right] \\ & - 8\lambda_1 E_0 \times \ln \left[\frac{\sqrt{X} + 4\lambda_1 E_0}{R + 2E_0} - \frac{16\lambda_1^2 + \frac{1}{J_0}}{8\lambda_1} \right] \Bigg\} + T_0 \end{aligned} \tag{30}$$

The application of SPM2 to 551 solar disturbance events of Solar Cycle 23 reveals that the success rates of SPM2 for both shock and nonshock events at Earth are slightly higher than 60%, and the prediction error for the shock events is within 12 h (root-mean-square) and 10 h (mean absolute), respectively. Table 1 gives a statistical comparison of a range of standard skill scores (from PODy to SR) derived by SPM2 with those derived by HAFv.2 based on 551 rather same events, with those by STOA on 463 same events, and with those by ISPM on 418 same events. These skill scores are introduced by the Fearless Forecast models from the meteorological forecasts in order to evaluate a model's prediction accuracy and reliability. The last two rows give the X^2 test for the model's prediction results. Higher values of X^2 and lower values of *p3* mean that the dependence between observations and predictions is stronger, and a value of $p3 < 0.05$ indicates a high level of significance. The "ideal value" of these parameters for the "perfect prediction" is also listed in the table. For these 11 skill scores from PODy to *p3*, SPM2 has at least nine scores better than any one of the Fearless Forecast models. Therefore, comparisons between the prediction results of SPM2 to those of STOA, ISPM, and HAFv.2 based on the same events demonstrate that the SPM2 model offers generally equivalent prediction accuracy and reliability; SPM2 provides better values for most of the evaluating skill scores than those Fearless Forecast models (STOA, ISPM, and HAFv.2).

Particularly, SPM2 has been developed to be an open-access online forecast tool on the website (http://www.spaceweather.ac.cn/groupmodel.php?group=sigma). The usage of the SPM2 forecast website is displayed in

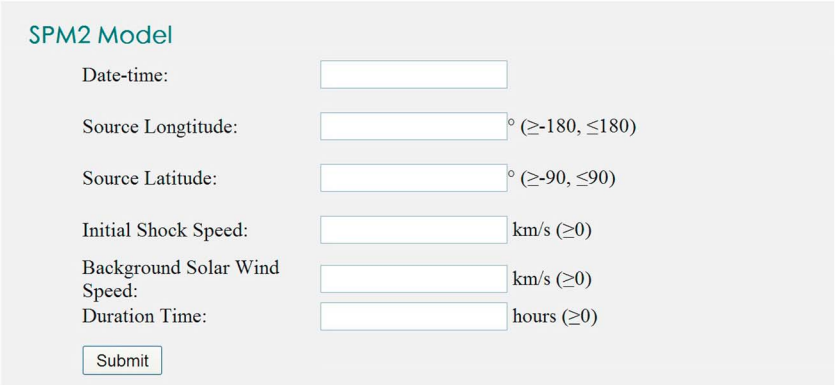

Figure 7. The online forecast tool based on SPM2.

Figure 7. Input parameters include the following: (1) the formation time (Date-time) of the shock near the Sun, usually denoted by the start time of type II bursts; (2) the source latitude (θ) and longitude (φ) in degrees in the heliographic coordinate system, often marked by the associated solar flare; (3) the initial shock speed (V_{si}) in km/s computed from the type II radio burst drifting speed; (4) the background solar wind speed (u_0) in km/s, which can be obtained from both solar wind models and in situ measurements of solar wind by L1 spacecraft near the shock's formation time; (5) the duration time (τ) in hours that refers to the piston-driving time duration of the shock (GOES X-ray duration as a proxy). The detailed introductions to these input parameters and their values for 551 events of Solar Cycle 23 can be found in *Zhao and Feng* [2014]. After filling in all the required input parameters, press the "Submit" button, then the webpage will output the prediction results of SPM2 immediately. For example, for the event happening at 22:10 UT on 14 December 2006 (Fearless Forecast No. 666), $\theta = -6°$, $\varphi = 46°$, $V_{si} = 1500$ km/s, $u_0 = 570$ km/s, $\tau = 2.0$ h, the prediction result is displayed as "The shock will arrive at the Earth at 2006-12-16 17:19:47. The transit time predicted is 43.16 hours!" on the webpage; For another event happening at 01:44 UT on 17 April 2005 (Fearless Forecast No. 592), $\theta = -12°$, $\varphi = -86°$, $V_{si} = 1003$ km/s, $u_0 = 400$ km/s, $\tau = 0.75$ h, and the prediction result is "The shock will not reach our Earth!."

2.5. Time-Dependent MHD Models

The physics-based magnetohydrodynamics (MHD) numerical models simulate the propagation process of solar disturbances in the background solar wind which is supplied by appropriate time-dependent boundary conditions near the Sun, and they can be used to give the predictions of solar disturbance's arrival time from the Sun to the Earth. Their success provides us confidence in the coming epoch of numerical space weather forecasting. There are a number of MHD models. For success and future improvements, *Feng et al.* [2011a, 2013a] provided the current status for the physics-based 3-D MHD space weather modeling. *Dryer* [2007] presented a modeler's perspective of the present state of the art for space weather simulation in 3-D MHD from the Sun to the Earth and beyond. Exhausting the significant body of literature already available in this context is beyond the scope of the present paper. Here only some typical 3-D models are briefly mentioned as examples.

The Space Weather Modeling Framework (SWMF) has been built by the Center for Space Environment Modeling at the University of Michigan and its collaborators [*Tóth et al.*, 2005, 2007, 2012]. As an ensemble of a sequence of MHD simulation models, SWMF includes several different models from the Sun to the Earth, i.e., Solar Corona (SC), Eruptive Event Generator (EE), Inner Heliosphere (IH), Solar Energetic Particles (SP), Global Magnetosphere (GM), Inner Magnetosphere (IM), Radiation Belt (RB), Ionosphere Electrodynamics (IE), and Upper Atmosphere (UA). The execution and parallel layout of the components is controlled by the SWMF, which supports both sequential and concurrent execution models. Adopting reasonably high spatial and temporal resolutions in all its coupled components, the SWMF runs significantly faster than real time on massively parallel supercomputers and enables those simulations that are impossible with the individual physics models to become feasible [*Tóth et al.*, 2005]. The SWMF could model different domains of the Sun-Earth system by combining different computational physics modules, and the subset of the modules can be used independently if needed. As far as the disturbance's arrival time prediction is concerned, only the models of SC, EE, and IH are involved. The simulation of the generation and propagation of CMEs runs about 2

times faster than real time on 256 CPUs of the Silicon Graphics Altix supercomputer Columbia and therefore can be used to give predictions in advance. The SWMF has been used to simulate the propagation of CMEs from the Sun to the Earth and reproduced successfully their arrival times and hydrodynamic characteristics for case studies [e.g., *Tóth et al.*, 2007; *Cohen et al.*, 2008; *Lugaz and Roussev*, 2011].

CORHEL (Coronal and Heliospheric) package is a coupled suite of solar corona and heliosphere models developed by the Center for Integrated Space weather Modeling [*Riley et al.*, 2012, 2013]. The corona models are composed of the Wang-Sheeley-Arge (WSA) and the MHD-Around-a-Sphere model, and the heliosphere model refers to the inner heliosphere solar wind model. The coupled WSA + ENLIL + Cone model, as one of the most sophisticated models currently available to space weather forecasters, is widely used to simulate the propagation and evolution of CMEs in interplanetary space and provides a 1–2 day lead time forecasting for major CMEs [*Taktakishvili et al.*, 2009, 2011; *Pizzo et al.*, 2011]. It is the combination of three models. WSA is a quasi-steady global solar wind model that uses synoptic magnetograms as inputs to predict ambient solar wind speed and interplanetary magnetic field polarity at Earth [*Wang and Sheeley*, 1995; *Arge and Pizzo*, 2000]. The ENLIL model, based on the polytropic equations of state for supersonic outflows, is a time-dependent, 3-D ideal MHD model of the solar wind in the heliosphere [*Odstrcil et al.*, 2002, 2004a, 2004b]. The Cone model is an empirical CME model based on the assumption that CMEs occupy the volume like a cone with constant angular width in the heliosphere [*Zhao et al.*, 2002; *Xie et al.*, 2004]. Although lacking the internal structure of CMEs, the Cone model has successfully simulated the propagation of CMEs and their impacts in the practice of MHD simulation [*Taktakishvili et al.*, 2009, 2011]. The input of ENLIL at its inner boundary of 21.5 R_s is taken from the output of WSA to get the background solar wind flows and interplanetary magnetic field. The observations of coronagraph for CMEs are used as input for the Cone model, whose output supplies the input for the transient CME structures required in the ENLIL model. *Zheng et al.* [2013] gave a brief description to the coupled WSA + ENLIL + Cone model as well as what had been learned about accurately modeling CMEs and their impacts based on the present space weather operations.

The Hybrid Heliospheric Modeling System (HHMS), developed by the Space Weather Predictions Center at the National Oceanic and Atmospheric Administration and its collaborators, is another Sun-to-Earth coupled modeling system that is composed of two physics-based models together with two simple empirical models [*Detman et al.*, 2006]. The physics-based models include a source surface (potential field) current sheet model for the corona and a time-dependent fully 3-D MHD model for the solar wind. The first empirical model is the empirical relationship between magnetic flux tube expansion factor and solar wind speed at 0.1 AU, and the second empirical model is used to predict the geomagnetic index based on the predicted solar wind at Earth as input. The HHMS has also the capability to simulate solar transient events such as CMEs and interplanetary shocks. *Smith et al.* [2008] compared the prediction ability of both HHMS and HAFv.2 for the arrival time at Earth of the solar-caused interplanetary shock of the 12 May 1997 solar event. It was found that HHMS could match better with the observations for the same inputs due to its updated solar surface observations to obtain a more reliable background solar wind. A newly developed hybrid model, called HAFv.2 + 3-DMHD, has been put forward by combining the HAFv.2 model with the 3-D MHD simulation code of the HHMS model [*Wu et al.*, 2007a, 2007b, 2011]. In this hybrid model, HAFv.2 is used from 2.5 R_s to 18 R_s (0.08 AU) to provide the input for the 3-D MHD code, which calculates the evolution of solar wind and interplanetary magnetic field beyond 0.08 AU. A dynamic disturbance is released into the quiescent solar wind structure to model the evolution and propagation of the solar transients (including both CME and shock) in the heliosphere. This hybrid model is found to be a useful tool to link CMEs at 1 AU to their solar sources, understand their propagations in interplanetary space, and also identify the possible origins of shock formation due to interaction between CMEs and CME/CIRs (Co-rotating Interaction Regions). The simulated solar wind parameters (density, velocity, magnetic field, and temperature) at 1 AU are verified by in situ observations of spacecraft.

The conservation element and solution element MHD (CESE MHD) [*Feng et al.*, 2007, 2010] models are full 3-D MHD models that can deal with the problems of solar wind ambient and solar disturbances from the Sun to the Earth developed by the Solar-Interplanetary-GeoMAgnetic (SIGMA) Weather Group, State Key Laboratory of Space Weather, Center for Space Science and Applied Research (CSSAR), Chinese Academy of Sciences. In contrast to conventional or other total variation diminishing type numerical schemes, time and space are treated as an entity in the CESE MHD models so that they avoid the calculation of eigenvalues and eigenvectors, which is a major difference from the traditional numerical methods. By mimicking CMEs with flux ropes, these

models are able to produce the propagation process of CMEs from the Sun to the Earth [e.g., *Zhou et al.*, 2012]. These CESE MHD models with continuously observed data as input exhibits the following innovative merits.

1. The new implementation of volumetric heating source term (*Feng et al.* [2010] and subsequent papers) that takes the topological effects of magnetic field, such as the expansion factor and the angular distance, into consideration, and can very effectively and realistically distinguish the high-speed solar wind from the low-speed solar wind [*Yang et al.*, 2011].
2. The introduction of composite grid strategies, such as six-component grid [*Feng et al.*, 2010, 2012a] and Yin-Yang grid [*Feng et al.*, 2011b], for the computational domain from the Sun to the Earth and beyond enables us to fit the spherical surface boundary with an easy implementation of the inner boundary conditions and meanwhile to avoid both coordinate singularities and polar grid convergence. Particularly, this feature allows us to easily use the solar observation as input data at the lower boundary thus conduct realistic, observation-based simulations.
3. In addition, the adaptive mesh refinement implementation of Solar-Interplanetary-CESE MHD (SIP-CESE MHD) model [*Feng et al.*, 2012a, 2012b, 2012c] in curvilinear coordinates (through the use of nonsingular transform from the physical space to the reference space) makes the code applicable to any coordinate system (such as Cartesian, spherical, cylindrical coordinates, and any other curvilinear coordinates) with only the difference of the coordinate transformations, and consequently, the solver is highly independent of the grid system thus applicable to many topics in solar physics and broad field in astrophysics and geophysics.
4. Time-dependent solar wind background study [*Feng et al.*, 2012a, 2012b, 2012c; *Yang et al.*, 2012] driven by daily updated solar observations and MHD evolution study of active regions [*Jiang and Feng*, 2013, *Jiang et al.*, 2013] driven by photospheric vector magnetogram, with the use of Wilcox Solar Observatory, SOHO/Michelson Doppler Imager, and Solar Dynamics Observatory/Helioseismic and Magnetic Imager observations, will open a new era for numerical space weather study both for time-dependent structured solar wind, the initiation process of solar eruptions, and their propagation in interplanetary space. The data-driven aspect of this methodology is unique in all 3-D MHD solar/interplanetary models: not only time-dependent B_r part but also including global surface flow. Including photospheric flux transport model with differential rotation and meridional flow is indeed an essential part to make a really realistic model [*Feng et al.*, 2012c].
5. Graphic Processing Unit implementation of CESE MHD model [*Feng et al.*, 2013b, 2013c] is aimed to speed up numerical space weather modeling for real-time operational forecasting purpose in order to combat the computer-intensive approach.

As suggested by *Feng et al.* [2012c, 2013c], in order to achieve better numerical results that can capture the structures of the heliosphere during specific time periods more accurately, high time-cadence photospheric magnetograms are needed to drive the model. Other considerations may include using synoptic maps from different observatories, choosing the solution that best matches the observations, and driving the numerical model by using the synoptic maps from the Air Force Data Assimilative Photospheric Flux Transport model [*Henney et al.*, 2012; *Lee et al.*, 2013], which can assimilate different observations into the surface flux model and thus provide more instantaneous snapshots of the global photospheric field distribution than traditional methods. At the same time, solar wind heating/acceleration needs further attention. As pointed out by *Feng et al.* [2010], further characterizing and quantifying of the key physical processes/mechanism will clarify an operational route to more physically integrate realistic coronal heating modules into 3-D MHD codes.

All these MHD models are milestones of the solar physics community in the world. Indeed, the observation-based realistic MHD simulation of the solar corona and solar wind is one of the hottest and most competitive topics in the solar physics community in the world, and inspiring researchers in the field of modeling of the solar corona and solar wind. With further long-term accumulation in the observations of solar eruptions and their propagation in the heliosphere as well as better understanding of the key physical processes/mechanisms in the solar wind heating/acceleration, validation of these MHD codes like CESE MHD model will, in our opinion, bring us into an operational capability for real-time solar disturbance arrival time prediction.

3. New Observations for Solar Disturbances in Solar Cycle 24

The launch of the STEREO in 2006 heralded a new epoch for the observations of solar eruptions and their related disturbances. In contrast with the earlier SOHO spacecraft, the observations of STEREO-A and STEREO-B

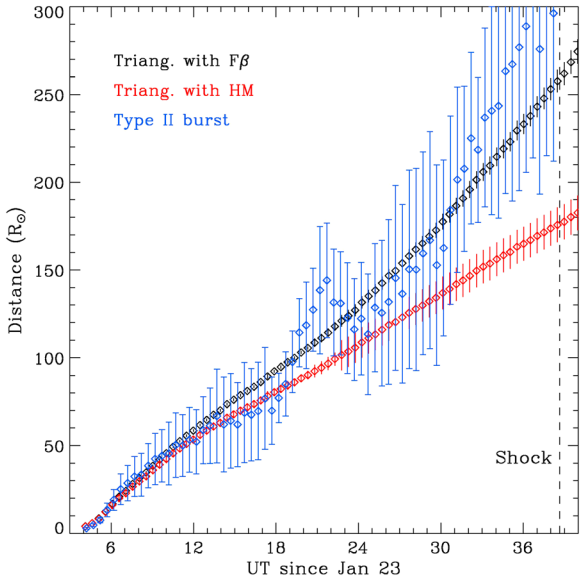

Figure 8. The variation of the leading edge distances for the 23 January 2012 CME event derived from Liu triangulation with Fβ (i.e., Fixed-φ, black), triangulation with HM (red), and the radio type II burst (blue). The vertical dashed line indicates the observed arrival time of the CME-driven shock at the Earth. Originally published in *Liu et al.* [2013].

greatly increase the community's ability in remote sensing tracking for solar disturbances in the following aspects: (1) two-point observations of STEREO make the 3-D reconstruction of solar eruptions become feasible, which are helpful in further understanding their morphologies and kinematics; (2) large FOV of the imaging telescopes (such as HI1 and HI2) enables the tracking of solar disturbances to much longer distance in the heliosphere, and this enlarges the ability of predicting arrival times of solar disturbances. A lot of techniques/models have been developed in these two aspects, such as the Point-P Method [*Howard et al.*, 2006; *Kahler and Webb*, 2007], Fixed-φ Method [*Kahler and Webb*, 2007; *Sheeley et al.*, 2008], Harmonic-Mean (HM) model [*Lugaz et al.*, 2009, 2010], Tappin-Howard Model [*Howard and Tappin*, 2009; *Tappin and Howard*, 2009], Tie-pointing Technique [*Srivastava et al.*, 2009; *Temmer et al.*, 2009], Inverse reconstruction [*Antunes et al.*, 2009], Geometric Localization technique [*De Koning et al.*, 2009], Graduated Cylindrical Shell forward modeling [*Thernisien et al.*, 2006, 2009], Local Correlation Tracking [*Mierla et al.*, 2009], Liu tracking [*Liu et al.*, 2010], Mask Fitting [*Feng et al.*, 2012], Ellipsoid Model [*Schreiner et al.*, 2012], Self-Similar Expansion model [*Davis et al.*, 2012; *Möstl and Davies*, 2013], and so on. Solar eruptions can be clearly tracked to much longer helio-distance based on the observation of STEREO than those on the observation of SOHO [e.g., *Zhao et al.*, 2010], even can be tracked to the Earth's orbit [*Liu et al.*, 2013]. Figure 8 displays the distance of the CME's leading edge distances plotted versus time for the 23 January 2012 event derived from the Liu tracking method. The CME was tracked beyond the Earth's distance in this case [*Liu et al.*, 2013]. These techniques/models can be used in empirical or analytical models to predict the 1 AU arrival time of solar disturbances [e.g., *Schreiner et al.*, 2012; *Möstl and Davies*, 2013], and the prediction accuracy would be greatly improved in contrast with those from models based on old observations. For example, Table 2 shows the arrival times at 1 AU of the CME's leading and trailing edges predicted by the Ellipsoid Model as well as comparisons with observations for three CMEs given by *Schreiner et al.* [2012]. The prediction error ranges from 0.4 to 6.2 h.

Although ranging from the highly complex and computationally intensive ones to those based on simple curve fitting, these techniques/models all have their inherent advantages and limitations [*Davis et al.*, 2012]. But they enlarge the community's understanding in the propagation and evolution of solar disturbances in the heliosphere, could be used to check the validity of previous models on arrival time prediction, and/or help to establish new models more close to the reality. However, studies in this aspect have only been carried

Table 2. The Predicted Beginning and End of the Ellipsoid's Transit Compared to the First Density Enhancement and the One Directly Following the Low-Density Cavity in the In Situ Data for Three CMEs, Respectively[a]

Event/Satellite	Predicted Arrival Time	In Situ Time	Hours Away	σ Away
1	12/30/07 4:56 ± 2:07	12/30/07 4:00 ± 3:00	0.95	0.26
ST-B	12/31/07 9:09 ± 3:17	12/31/07 3:00 ± 0:45	6.16	1.83
2	4/29/08 19:12 ± 1:38	4/29/08 14:45 ± 0:45	4.46	2.47
ST-B	4/29/08 21:08 ± 2:05	4/29/08 18:15 ± 1:00	2.90	1.25
3	12/15/08 6:45 ± 0:20	12/15/08 4:30 ± 3:00	2.26	0.75
WIND	12/17/08 17:41 ± 1:08	12/17/08 17:15 ± 3:00	0.44	0.14

[a]Adapted from *Schreiner et al.* [2012], with redrawing.

out for case studies, which are not based on a large number of data sets. The reason for this may be the extremely low level of solar activity of the present solar cycle. A large number of data sets of solar disturbance events have not been built up in Solar Cycle 24 as those collected in Solar Cycle 23. And this will be improved as more solar eruptions are observed in the future.

4. Summary and Discussion

The current status of the CME/shock arrival time prediction models is reviewed in this paper according to the classification of empirical models, expansion speed model, drag-based models, physics-based models, and MHD models. This is not an exhaustive review for all the models in this aspect, and more descriptions can be found in similarly summarized papers [e.g., *Owens and Cargill*, 2004; *Siscoe and Schwenn*, 2006; *Watermann et al.*, 2009; *Davis et al.*, 2011; *Zheng et al.*, 2013]. Although some models are very complicated and considerate while others are rather simple and easy, no great gaps are found between their prediction capabilities and accuracies. In other words, no model is evidently better than the others. The predictions yield generally 12 h in the root-mean-square error and 10 h in the mean absolute error for a large number of data events. Some models claim that their prediction errors are dramatically smaller than this average error, but they are applied only for case studies. Better prediction of solar disturbance's propagation and arrival time requires an improved understanding of both the disturbance and the medium that they travel through. There are many factors impeding further improvements of present models. (1) The input parameters of the model have their own uncertainties. For example, the CME speeds observed by coronagraphs are the speeds projected on the plane of sky, and their Earth-directed speeds cannot be obtained in the SOHO era. Even for the observations of STEREO, the 3-D reconstructions of CMEs still require inevitable assumptions and simplifications. (2) The knowledge of 3-D morphology and kinematics of solar disturbance is still limited. Any model will have its deficiency in depicting the real complicated solar transients. The blast wave theory may not be suitable for the extremely slow speed eruptions and their driven waves, while piston-driven theory should not be the best candidate to describe the motion of very fast CME/shocks. (3) The real background solar wind that the disturbance travels through is difficult to be either observed (should be known, temporally, in 3-D before their arrivals) or simulated from MHD or empirical models. But the evident influence of the ambient solar wind on the disturbance's propagation and arrival time is accepted by all the prediction models. (4) Many other factors also have great effects on the arrival time of solar disturbance such as the deviations in their propagation, the solar wind inhomogeneities and fluctuations [*Heinemann*, 2002], the large-scale structure of the heliospheric current sheet [*Zhao et al.*, 2007], the interactions between transients and other structures, and some other, as yet unknown, factors. These factors are difficult to be considered together in one operational model. Along with the progress in the observations of solar and interplanetary transients as well as the maturity of 3-D MHD models [*Feng et al.*, 2011a, 2013a], these issues could be solved step by step. Accurate predictions for both the arrival time and the time-dependent evolution of the structures of solar transients will be fulfilled in the future.

Acknowledgments

This work is jointly supported by the National Basic Research Program (973 program) under grant 012CB825601, the Knowledge Innovation Program of the Chinese Academy of Sciences (KZZD-EW-01-4), the National Natural Science Foundation of China (41031066, 41231068, 41274179, 41274192, and 41374176), and the Specialized Research Fund for State Key Laboratories. We thank the reviewers for their helpful comments and suggestions.

References

Antunes, A., A. Thernisien, and A. Yahil (2009), Hybrid reconstruction to derive 3D height-time evolution for coronal mass ejections, *Sol. Phys.*, *259*, 199–212.

Aran, A., B. Sanahuja, and D. Lario (2006), SOLPENCO: A solar particle engineering code, *Adv. Space Res.*, *37*, 1240–1246.

Arge, C. N., and V. J. Pizzo (2000), Improvement in the prediction of solar wind conditions using near-real time solar magnetic field updates, *J. Geophys. Res.*, *105*(A5), 10,465–10,479, doi:10.1029/1999JA000262.

Boteler, D. H., R. J. Pirjola, and H. Nevanlinna (1998), The effects of geomagnetic disturbances on electrical systems at the Earth's surface, *Adv. Space Res.*, *22*, 17–27.

Brueckner, G. E., J.-P. Delaboudiniere, R. A. Howard, S. E. Paswaters, O. C. St. Cyr, R. Schwenn, P. Lamy, G. M. Simnett, B. Thompson, and D. Wang (1998), Geomagnetic storms caused by coronal mass ejections (CMEs): March 1996 through June 1997, *Geophys. Res. Lett.*, *25*(15), 3019–3022, doi:10.1029/98GL00704.

Cargill, P. J. (2004), On the aerodynamic drag force acting on interplanetary coronal mass ejections, *Sol. Phys.*, *221*, 135–149.

Cargill, P. J., J. Chen, D. S. Spicer, and S. T. Zalesak (1996), Magnetohydrodynamic simulations of the motion of magnetic flux tubes through a magnetized plasma, *J. Geophys. Res.*, *101*(A3), 4855–4870, doi:10.1029/95JA03769.

Cliver, E. W., and A. G. Ling (2009), Low-frequency type III bursts and solar energetic particle events, *Astrophys. J.*, *690*, 598–609.

Cohen, O., I. V. Sokolov, I. I. Roussev, N. Lugaz, W. B. Manchester, T. I. Gombosi, and C. N. Arge (2008), Validation of a global 3D heliospheric model with observations for the May 12, 1997 CME event, *J. Atmos. Sol. Terr. Phys.*, *70*, 583–592.

Davis, C. J., et al. (2011), A comparison of space weather analysis techniques used to predict the arrival of the Earth-directed CME and its shockwave launched on 8 April 2010, *Space Weather*, *9*, S01005, doi:10.1029/2010SW000620.

Davis, J. A., et al. (2012), A self-similar expansion model for use in solar wind transient propagation studies, *Astrophys. J.*, *750*(23), 12, doi:10.1088/0004-637X/750/1/23.

De Koning, C. A., V. J. Pizzo, and D. A. Biesecker (2009), Geometric localization of CMEs in 3D space using STEREO beacon data: First results, *Sol. Phys.*, *256*, 167–181.
Detman, T., Z. Smith, M. Dryer, C. D. Fry, C. N. Arge, and V. Pizzo (2006), A hybrid heliospheric modeling system: Background solar wind, *J. Geophys. Res.*, *111*, A07102, doi:10.1029/2005JA011430.
Dryer, M. (1974), Interplanetary shock waves generated by solar flares, *Space Sci. Rev.*, *15*, 403–468.
Dryer, M. (2007), Space weather simulation in 3D MHD from the Sun to the Earth and beyond to 100 AU: A modeler's perspective of the present state of the art, *Asian J. Phys*, *16*, 97–121.
Dryer, M., and D. F. Smart (1984), Dynamical models of coronal transients and interplanetary disturbances, *Adv. Space Res.*, *4*, 291–301.
Dryer, M., C. D. Fry, W. Sun, C. S. Deehr, Z. Smith, S.-I. Akasofu, and M. D. Andrews (2001), Prediction in real-time of the 2000 July 14 heliospheric shock wave and its companions during the "Bastille" epoch, *Sol. Phys.*, *204*, 265–284.
Dryer, M., Z. Smith, C. D. Fry, W. Sun, C. S. Deehr, and S.-I. Akasofu (2004), Real-time shock arrival predictions during the "Halloween 2003" epoch, *Space Weather*, *2*, S09001, doi:10.1029/2004SW000087.
Feng, L., B. Inhester, Y. Wei, W. Q. Gan, T. L. Zhang, and M. Y. Wang (2012), Morphological evolution of a three-dimensional coronal mass ejection cloud reconstructed from three viewpoints, *Astrophys. J.*, *751*(18), 12.
Feng, X. S., and X. H. Zhao (2006), A new prediction method for the arrival time of interplanetary shocks, *Sol. Phys.*, *238*, 167–186.
Feng, X. S., Y. F. Zhou, and S. T. Wu (2007), A novel numerical implementation for solar wind modeling by the modified conservation element/solution element method, *Astrophys. J.*, *655*, 1110–1126.
Feng, X. S., Y. Zhang, W. Sun, M. Dryer, C. D. Fry, and C. S. Deehr (2009), A practical database method for predicting arrivals of "average" interplanetary shocks at Earth, *J. Geophys. Res.*, *114*, A01101, doi:10.1029/2008JA013499.
Feng, X. S., L. P. Yang, C. Q. Xiang, S. T. Wu, Y. F. Zhou, and D. K. Zhong (2010), Three-dimensional solar wind modeling from the Sun to Earth by a SIP-CESE MHD Model with a six-component grid, *Astrophys. J.*, *723*, 300–319.
Feng, X. S., C. Q. Xiang, and D. K. Zhong (2011a), The state-of-art of three-dimensional numerical study for corona-interplanetary process of solar storms [in Chinese], *Sci. Sin-Terrae*, *41*, 1–28.
Feng, X. S., S. H. Zhang, C. Q. Xiang, L. P. Yang, C. W. Jiang, and S. T. Wu (2011b), A hybrid solar wind model of the CESE+HLL method with a Yin-Yang overset grid and an AMR grid, *Astrophys. J.*, *734*(50), 11.
Feng, X. S., L. P. Yang, C. Q. Xiang, C. W. Jiang, X. P. Ma, S. T. Wu, D. K. Zhong, and Y. F. Zhou (2012a), Validation of the 3D AMR SIP–CESE solar wind model for four Carrington rotations, *Sol. Phys.*, *279*, 207–229, doi:10.1007/s11207-012-9969-9.
Feng, X. S., L. P. Yang, C. Q. Xiang, Y. Liu, X. Zhao, and S. T. Wu (2012b), Numerical study of the global corona for CR 2055 driven by daily updated synoptic magnetic field, in *Numerical Modeling of Space Plasma Flows (Astronum 2011)*, *ASP Conf. Ser*, vol. 459, edited by N. V. Pogorelov, J. A. Font, and E. Audit, pp. 202–208, Astronomical Society of the Pacific, San Francisco, Valencia, Spain.
Feng, X. S., C. W. Jiang, C. Q. Xiang, X. P. Zhao, and S. T. Wu (2012c), A data-driven model for the global coronal evolution, *Astrophys. J.*, *758*(62), 13.
Feng, X. S., C. Q. Xiang, and D. K. Zhong (2013a), Numerical study of interplanetary solar storms [in Chinese], *Sci. Sin. Terrae*, *43*, 912–933.
Feng, X. S., D. K. Zhong, C. Q. Xiang, and Y. Zhang (2013b), GPU computing in Space Weather Modeling, in *Numerical Modeling of Space Plasma Flows (Astronum 2012), ASP Conf. Ser.*, vol. 474, edited by N. V. Pogorelov, E. Audit, and G. P. Zank, pp. 131–139, Astronomical Society of the Pacific, San Francisco, Calif.
Feng, X. S., D. K. Zhong, C. Q. Xiang, and Y. Zhang (2013c), GPU-accelerated computing of three-dimensional solar wind background, *Sci. China Earth Sci.*, *56*, 1864–1880, doi:10.1007/s11430-013-4661-y.
Fry, C. D., W. Sun, C. S. Deehr, M. Dryer, Z. Smith, S.-I. Akasofu, M. Tokumaru, and M. Kojima (2001), Improvements to the HAF solar wind model for space weather predictions, *J. Geophys. Res.*, *106*, 20,985–21,001, doi:10.1029/2000JA000220.
Fry, C. D., M. Dryer, Z. Smith, W. Sun, C. S. Deehr, and S.-I. Akasofu (2003), Forecasting solar wind structures and shock arrival times using an ensemble of models, *J. Geophys. Res.*, *108*(A2), 1070, doi:10.1029/2002JA009474.
Fry, C. D., T. R. Detman, M. Dryer, Z. Smith, W. Sun, C. S. Deehr, S.-I. Akasofu, C.-C. Wu, and S. McKenna-Lawlor (2007), Real time solar wind forecasting: Capabilities and challenges, *J. Atmos. Sol. Terr. Phys.*, *69*, 109–115.
Gopalswamy, N., A. Lara, R. P. Lepping, M. L. Kaiser, D. Berdichevsky, and O. C. St. Cyr (2000), Interplanetary acceleration of coronal mass ejections, *Geophys. Res. Lett.*, *27*(2), 145–148, doi:10.1029/1999GL003639.
Gopalswamy, N., A. Lara, S. Yashiro, M. L. Kaiser, and R. A. Howard (2001), Predicting the 1-AU arrival times of coronal mass ejections, *J. Geophys. Res.*, *106*(A12), 29,207–29,217, doi:10.1029/2001JA000177.
Gopalswamy, N., S. Yashiro, A. Lara, M. L. Kaiser, B. J. Thompson, P. T. Gallagher, and R. A. Howard (2003), Large solar energetic particle events of cycle 23: A global view, *Geophys. Res. Lett.*, *30*(12), 8015, doi:10.1029/2002GL016435.
Gopalswamy, N., A. Lara, P. K. Manoharan, and R. A. Howard (2005), An empirical model to predict the 1-AU arrival of interplanetary shocks, *Adv. Space Res.*, *36*, 2289–2294.
Gopalswamy, N., P. Mäkelä, H. Xie, and S. Yashiro (2013), Testing the empirical shock arrival model using quadrature observations, *Space Weather*, *11*, 661–669, doi:10.1002/2013SW000945.
Gosling, J. T., D. J. McComas, J. L. Phillips, and S. J. Bame (1991), Geomagnetic activity associated with Earth passage of interplanetary shock disturbances and coronal mass ejections, *J. Geophys. Res.*, *96*, 7831–7839, doi:10.1029/91JA00316.
Heinemann, M. (2002), Effects of solar wind inhomogeneities on transit times of interplanetary shock waves, *J. Atmos. Sol. Terr. Phys.*, *64*, 315–325.
Henney, C. J., W. A. Toussaint, S. M. White, and C. N. Arge (2012), Forecasting $F_{10.7}$ with solar magnetic flux transport modeling, *Space Weather*, *10*, S02011, doi:10.1029/2011SW000748.
Howard, T. A., and S. J. Tappin (2005), Statistical survey of earthbound interplanetary shocks, associated coronal mass ejections and their space weather consequences, *Astron. Astrophys.*, *440*, 373–383.
Howard, T. A., and S. J. Tappin (2009), Interplanetary coronal mass ejections observed in the heliosphere. 1. Review of theory, *Space Sci. Rev.*, *147*, 31–54.
Howard, T. A., D. F. Webb, S. J. Tappin, D. R. Mizuno, and J. C. Johnston (2006), Tracking halo coronal mass ejections from 0-1 AU and space weather forecasting using the Solar Mass Ejection Imager (SMEI), *J. Geophys. Res.*, *111*, A04105, doi:10.1029/2005JA011349.
Hudson, H. S., J.-L. Bougeret, and J. Burkepile (2006), Coronal mass ejections: Overview of observations, *Space Sci. Rev.*, *123*, 13–30.
Hundhausen, A. J., C. B. Sawyer, L. House, R. M. E. Illing, and W. J. Wagner (1984), Coronal mass ejections observed during the solar maximum mission - Latitude distribution and rate of occurrence, *J. Geophys. Res.*, *89*(18), 2639–2646, doi:10.1029/JA089iA05p02639.
Jiang, C. W., and X. S. Feng (2013), Extrapolation of the solar coronal magnetic field from SDO/HMI magnetogram by a CESE-MHD-NLFFF code, *Astrophys. J.*, *769*(144), 13, doi:10.1088/0004-637X/769/2/144.

Jiang, C. W., X. S. Feng, S. T. Wu, and Q. Hu (2013), Magnetohydrodynamic simulation of a sigmoid eruption of active region 11283, *Astrophys. J. Lett.*, *771*(L30), 5, doi:10.1088/2041-8205/771/2/L30.
Kahler, S. W., and D. F. Webb (2007), V arc interplanetary coronal mass ejections observed with the Solar Mass Ejection Imager, *J. Geophys. Res.*, *112*, A09103, doi:10.1029/2007JA012358.
Kim, K.-H., Y.-J. Moon, and K.-S. Cho (2007), Prediction of the 1 AU arrival times of CME-associated interplanetary shocks: Evaluation of an empirical interplanetary shock propagation model, *J. Geophys. Res.*, *112*, A05104, doi:10.1029/2006JA011904.
Lanzerotti, L. J. (2005), High-energy solar particles and human explorations, *Space Weather*, *3*, S05002, doi:10.1029/2005SW000174.
Lee, C. O., C. N. Arge, D. Odstrčil, G. Millward, V. Pizzo, J. M. Quinn, and C. J. Henney (2013), Ensemble modeling of CME propagation, *Sol. Phys.*, *285*, 349–368, doi:10.1007/s11207-012-9980-1.
Li, H. J., F. S. Wei, X. S. Feng, and Y. Q. Xie (2008), On improvement to the Shock Propagation Model (SPM) applied to interplanetary shock transit time forecasting, *J. Geophys. Res.*, *113*, A09101, doi:10.1029/2008JA013167.
Liu, H.-L., and G. Qin (2012), Using soft X-ray observations to help the prediction of flare related interplanetary shocks arrival times at the Earth, *J. Geophys. Res.*, *117*, A04108, doi:10.1029/2011JA017220.
Liu, Y. D., J. G. Luhmann, N. Lugaz, C. Möstl, J. A. Davies, S. D. Bale, and R. P. Lin (2013), On Sun-to-Earth propagation of coronal mass ejections, *Astrophys. J.*, *769*(45), 15.
Liu, Y., J. A. Davies, J. G. Luhmann, A. Vourlidas, S. D. Bale, and R. P. Lin (2010), Geometric triangulation of imaging observations to track coronal mass ejections continuously out to 1 AU, *Astrophys. J. (Letters)*, *710*, L82–L87.
Lugaz, N., and I. I. Roussev (2011), Numerical modeling of interplanetary coronal mass ejections and comparison with heliospheric images, *J. Atmos. Sol. Terr. Phys.*, *73*, 1187–1200.
Lugaz, N., A. Vourlidas, and I. I. Roussev (2009), Deriving the radial distances of wide coronal mass ejections from elongation measurements in the heliosphere - Application to CME-CME interaction, *Ann. Geophys.*, *27*, 3479–3488.
Lugaz, N., J. N. Hernandez-Charpak, I. I. Roussev, C. J. Davis, A. Vourlidas, and J. A. Davis (2010), Determining the azimuthal properties of coronal mass ejections from multi-spacecraft remote-sensing observations with STEREO SECCHI, *Astrophys. J.*, *715*, 493–499.
Manoharan, P. K. (2006), Evolution of coronal mass ejections in the inner heliosphere: A study using white-light and scintillation images, *Sol. Phys.*, *235*, 345–368.
Manoharan, P. K., M. Kojima, N. Gopalswamy, T. Kondo, and Z. Smith (2000), Radial evolution and turbulence characteristics of a coronal mass ejection, *Astrophys. J.*, *530*, 1061–1070.
Manoharan, P. K., N. Gopalswamy, S. Yashiro, A. Lara, G. Michalek, and R. A. Howard (2004), Influence of coronal mass ejection interaction on propagation of interplanetary shocks, *J. Geophys. Res.*, *109*, A06109, doi:10.1029/2003JA010300.
McKenna-Lawlor, S. M. P., M. Dryer, Z. Smith, K. Kecskemety, C. D. Fry, W. Sun, C. S. Deehr, D. Berdichevsky, K. Kudela, and G. Zastenker (2002), Arrival times of flare/halo CME associated shocks at the Earth: Comparison of the predictions of three numerical models with these observations, *Ann. Geophys.*, *20*, 917–935.
McKenna-Lawlor, S. M. P., M. Dryer, M. D. Kartalev, Z. Smith, C. D. Fry, W. Sun, C. S. Deehr, K. Kecskemety, and K. Kudela (2006), Near real-time predictions of the arrival at Earth of flare related shocks during Solar Cycle 23, *J. Geophys. Res.*, *111*, A11103, doi:10.1029/2005JA011162.
McKenna-Lawlor, S. M. P., C. D. Fry, M. Dryer, D. Heynderickx, K. Kecskemety, K. Kudela, and J. Balaz (2012), A statistical study of the performance of the Hakamada-Akasofu-Fry version 2 numerical model in predicting solar shock arrival times at Earth during different phases of solar cycle 23, *Ann. Geophys.*, *30*, 405–419.
Michalek, G., N. Gopalswamy, and S. Yashiro (2008), Space weather application using projected velocity asymmetry of halo CMEs, *Sol. Phys.*, *248*, 113–123, doi:10.1007/s11207-008-9126-7.
Mierla, M., B. Inhester, C. Marqué, L. Rodriguez, S. Gissot, A. N. Zhukov, D. Berghmans, and J. Davila (2009), On 3D reconstruction of coronal mass ejections: I. Method description and application to SECCHI-COR data, *Sol. Phys.*, *259*, 123–141.
Moon, Y. J., M. Dryer, Z. Smith, Y. D. Park, and K. S. Cho (2002), A revised shock time of arrival (STOA) model for interplanetary shock propagation: STOA-2, *Geophys. Res. Lett.*, *29*(10), 1390, doi:10.1029/2002GL014865.
Möstl, C., and J. A. Davies (2013), Speeds and arrival times of solar transients approximated by self-similar expanding circular fronts, *Sol. Phys.*, *285*, 411–423.
Odstrcil, D., J. A. Linker, R. Lionello, Z. Mikic, P. Riley, V. J. Pizzo, and J. G. Luhmann (2002), Merging of coronal and heliospheric two-dimensional MHD models, *J. Geophys. Res.*, *107*(A12), 1493, doi:10.1029/2002JA009334.
Odstrcil, D., V. J. Pizzo, J. A. Linker, P. Riley, R. Lionello, and Z. Mikic (2004a), Initial coupling of coronal and heliospheric numerical magnetohydrodynamic codes, *J. Atmos. Sol. Terr. Phys.*, *66*, 1311–1320.
Odstrcil, D., P. Riley, and X. P. Zhao (2004b), Numerical simulation of the 12 May 1997 interplanetary CME event, *J. Geophys. Res.*, *109*, A02116, doi:10.1029/2003JA010135.
Owens, M., and P. Cargill (2004), Predictions of the arrival time of coronal mass ejections at 1 AU: An analysis of the causes of errors, *Ann. Geophys.*, *22*, 661–671.
Payne-Scott, R., D. E. Yabsley, and J. G. Bolton (1947), Relative times of arrival of bursts of solar noise on different radio frequencies, *Nature*, *160*, 256–257.
Pizzo, V., G. Millward, A. Parsons, D. Biesecker, S. Hill, and D. Odstrcil (2011), Wang-Sheeley-Arge–Enlil cone model transitions to operations, *Space Weather*, *9*, S03004, doi:10.1029/2011SW000663.
Qin, G., M. Zhang, and H. K. Rassoul (2009), Prediction of the shock arrival time with SEP observations, *J. Geophys. Res.*, *114*, A09104, doi:10.1029/2009JA014332.
Reiner, M. J., M. L. Kaiser, and J.-L. Bougeret (2007), Coronal and interplanetary propagation of CME/shocks from radio, in situ and white-light observations, *Astrophys. J.*, *663*, 1369–1385.
Riley, P., J. A. Linker, R. Lionello, and Z. Mikić (2012), Corotating interaction regions during the recent solar minimum: The power and limitations of global MHD modeling, *J. Atmos. Sol. Terr. Phys.*, *83*, 1–10.
Riley, P., J. A. Linker, and Z. Mikić (2013), On the application of ensemble modeling techniques to improve ambient solar wind models, *J. Geophys. Res. Space Physics*, *118*, 600–607, doi:10.1002/jgra.50156.
Schreiner, S., C. Cattell, K. Kersten, and A. Hupach (2012), Using an ellipsoid model to track and predict the evolution and propagation of coronal mass ejections, *Sol. Phys.*, doi:10.1007/s11207-012-9936-5.
Schwenn, R., A. Dal Lago, E. Huttunen, and W. D. Gonzalez (2005), The association of coronal mass ejections with their effects near the Earth, *Ann. Geophys.*, *23*(3), 1033–1059.
Shanmugaraju, A., and B. Vršnak (2014), Transit time of coronal mass ejections under different ambient solar wind conditions, *Sol. Phys.*, *289*, 339–349.

Sheeley, N. R., Jr., R. A. Howard, M. J. Koomen, D. J. Michels, R. Schwenn, K. H. Mühlhäuser, and H. Rosenbauer (1985), Coronal mass ejections and interplanetary shocks, *J. Geophys. Res.*, *90*(A1), 163–175, doi:10.1029/JA090iA01p00163.
Sheeley, N. R., et al. (1997), Measurements of flow speeds in the corona between 2 and 30 $R_{\odot}$, *Astrophys. J.*, *484*, 472–478.
Sheeley, N. R., et al. (2008), Heliospheric images of the solar wind at Earth, *Astrophys. J.*, *675*, 853–862.
Siscoe, G., and R. Schwenn (2006), CME disturbance forecasting, *Space Sci. Rev.*, *123*, 453–470.
Smart, D. F., and M. A. Shea (1984), A simplified technique for estimating the arrival time of solar flare-initiated shocks, in *Proc. STIP Workshop on Solar/Interplanetary Intervals*, edited by M. A. Shea, D. F. Smart, and S. McKenna-Lawlor, pp. 139–256, Publ. Book Crafters, Chelsea, Michigan.
Smart, D. F., and M. A. Shea (1985), A simplified model for timing the arrival of solar flare-initiated shocks, *J. Geophys. Res.*, *90*, 183–190, doi:10.1029/JA090iA01p00183.
Smith, Z. K., and W. J. Murtagh (2009), Solar wind low-energy energetic ion enhancements: A tool to forecast large geomagnetic storms, *Adv. Space Res.*, *44*, 775–788.
Smith, Z. K., W. Murtagh, and C. Smithtro (2004), Relationship between solar wind low-energy energetic ion enhancements and large geomagnetic storms, *J. Geophys. Res.*, *109*, A01110, doi:10.1029/2003JA010044.
Smith, Z. K., T. R. Detman, W. Sun, M. Dryer, C. S. Deehr, and C. D. Fry (2008), Modeling the arrival at Earth of the interplanetary shock following the 12 May 1997 solar event using HAFv2 and 3-D MHD HHMS models, *Space Weather*, *6*, S05006, doi:10.1029/2007SW000356.
Smith, Z. K., M. Dryer, S. M. P. McKenna-Lawlor, C. D. Fry, C. S. Deehr, and W. Sun (2009a), Operational validation of HAFv2's predictions of interplanetary shock arrivals at Earth: Declining phase of Solar Cycle 23, *J. Geophys. Res.*, *114*, A05106, doi:10.1029/2008JA013836.
Smith, Z. K., R. Steenburgh, C. D. Fry, and M. Dryer (2009b), Predictions of interplanetary shock arrivals at Earth: Dependence of forecast outcome on the input parameters, *Space Weather*, *7*, S12005, doi:10.1029/2009SW000500.
Smith, Z., and M. Dryer (1990), MHD study of temporal and spatial evolution of simulated interplanetary shocks in the ecliptic plane within 1 AU, *Sol. Phys.*, *129*, 387–405.
Smith, Z., and M. Dryer (1995), The interplanetary shock propagation model: A model for predicting solar-flare-caused geomagnetic storms, based on the 2 1/2D MHD numerical simulation results from the interplanetary global model, NOAA technical memorandum ERL/SEL-89, July.
Smith, Z., M. Dryer, and C. D. Fry (2005), Determining shock velocities for inputs to Sun-to-Earth models from radio and coronagraph data, *Space Weather*, *3*, S07002, doi:10.1029/2004SW000136.
Song, W. B. (2010), An analytical model to predict the arrival time of interplanetary CMEs, *Sol. Phys.*, *261*, 311–320.
Srivastava, N., and P. Venkatakrishnan (2004), Solar and interplanetary sources of major geomagnetic storms during 1996–2002, *J. Geophys. Res.*, *109*, A10103, doi:10.1029/2003JA010175.
Srivastava, N., B. Inhester, M. Mierla, and B. Podlipnik (2009), 3D reconstruction of the leading edge of the May 20, 2007 partial halo CME, *Sol. Phys.*, *259*, 213–225.
Subramanian, P., A. Lara, and A. Borgazzi (2012), Can solar wind viscous drag account for coronal mass ejection deceleration?, *Geophys. Res. Lett.*, *39*, L19107, doi:10.1029/2012GL053625.
Sun, W., M. Dryer, C. D. Fry, C. S. Deehr, Z. Smith, S.-I. Akasofu, M. D. Kartalev, and K. G. Grigorov (2002), Evaluation of solar type II radio burst estimates of initial solar wind shock speed using a kinematic model of the solar wind on the April 2001 solar wind swarm, *Geophys. Res. Lett.*, *29*(8), 1171, doi:10.1029/2001GL013659.
Sun, W., C. S. Deehr, C. D. Fry, M. Dryer, Z. Smith, and S.-I. Akasofu (2003), Plane-of-sky simulations of interplanetary shock waves, *Geophys. Res. Lett.*, *30*(20), 2044, doi:10.1029/2003GL017574.
Taktakishvili, A., M. Kuznetsova, P. MacNeice, M. Hesse, L. Rastätter, A. Pulkkinen, A. Chulaki, and D. Odstrcil (2009), Validation of the coronal mass ejection predictions at the Earth orbit estimated by ENLIL heliosphere cone model, *Space Weather*, *7*, S03004, doi:10.1029/2008SW000448.
Taktakishvili, A., A. Pulkkinen, P. MacNeice, M. Kuznetsova, M. Hesse, and D. Odstrcil (2011), Modeling of coronal mass ejections that caused particularly large geomagnetic storms using ENLIL heliosphere cone model, *Space Weather*, *9*, S06002, doi:10.1029/2010SW000642.
Tappin, S. J., and T. A. Howard (2009), Interplanetary coronal mass ejections observed in the heliosphere. 2. Model and data comparison, *Space Sci. Rev.*, *147*, 55–87.
Temmer, M., S. Preiss, and A. M. Veronig (2009), CME projection effects studied with STEREO/COR and SOHO/LASCO, *Sol. Phys.*, *256*, 183–199.
Thernisien, A. F. R., R. A. Howard, and A. Vourlidas (2006), Modeling of flux rope coronal mass ejections, *Astrophys. J.*, *652*, 763–773.
Thernisien, A., A. Vourlidas, and R. A. Howard (2009), Forward modeling using STEREO/SECCHI data, *Sol. Phys.*, *256*, 111–130.
Tóth, G., et al. (2005), Space Weather Modeling Framework: A new tool for the space science community, *J. Geophys. Res.*, *110*, A12226, doi:10.1029/2005JA011126.
Tóth, G., D. L. de Zeeuw, T. I. Gombosi, W. B. Manchester, A. J. Ridley, I. V. Sokolov, and I. I. Roussev (2007), Sun-to-thermosphere simulation of the 28–30 October 2003 storm with the space weather modeling framework, *Space Weather*, *5*, S06003, doi:10.1029/2006SW000272.
Tóth, G., et al. (2012), Adaptive numerical algorithms in space weather modeling, *J. Comput. Phys.*, *231*, 870–903.
Vandas, M., S. Fischer, M. Dryer, Z. Smith, and T. Detman (1996), Parametric study of loop-like magnetic cloud propagation, *J. Geophys. Res.*, *101*(A7), 15,645–15,652, doi:10.1029/96JA00511.
Vršnak, B. (2001), Deceleration of coronal mass ejections, *Sol. Phys.*, *202*, 173–189.
Vršnak, B., and N. Gopalswamy (2002), Influence of the aerodynamic drag on the motion of interplanetary ejecta, *J. Geophys. Res.*, *107*(A2), 1019, doi:10.1029/2001JA000120.
Vršnak, B., and T. Žic (2007), Transit times of interplanetary coronal mass ejections and the solar wind speed, *Astron. Astrophys.*, *472*, 937–943.
Vršnak, B., T. Žic, T. V. Falkenberg, C. Möstl, S. Vennerstrom, and D. Vrbanec (2010), The role of aerodynamic drag in propagation of interplanetary coronal mass ejections, *Astron. Astrophys.*, *512*, A43, doi:10.1051/0004-6361/200913482.
Vršnak, B., et al. (2013), Propagation of interplanetary coronal mass ejections: The drag-based model, *Sol. Phys.*, *285*, 295–315.
Wang, Y. M., and N. R. Sheeley Jr. (1995), Solar implications of Ulysses interplanetary field measurements, *Astrophys. J.*, *447*, L143–L146.
Wang, Y. M., P. Z. Ye, S. Wang, G. P. Zhou, and J. X. Wang (2002), A statistical study on the geoeffectiveness of Earth-directed coronal mass ejections from March 1997 to December 2000, *J. Geophys. Res.*, *107*(A11), 1340, doi:10.1029/2002JA009244.
Watermann, J., et al. (2009), Models of solar wind structures and their interaction with the Earth's space environment, *Space Sci. Rev.*, *147*, 233–270, doi:10.1007/s11214-009-9494-9.
Wei, F. S. (1982), The blast wave propagation in a moving medium with variable density, *Chin. J. Space Sci.*, *2*, 63–72.
Wei, F. S., and M. Dryer (1991), Propagation of solar flare-associated interplanetary shock waves in the heliospheric meridional plane, *Sol. Phys.*, *132*, 373–394.
Wu, C.-C., C. D. Fry, S. T. Wu, M. Dryer, and K. Liou (2007a), Three-dimensional global simulation of interplanetary coronal mass ejection propagation from the Sun to the heliosphere: Solar event of 12 May 1997, *J. Geophys. Res.*, *112*, A09104, doi:10.1029/2006JA012211.
Wu, C.-C., C. D. Fry, M. Dryer, S. T. Wu, B. Thompson, K. Liou, and X. S. Feng (2007b), Three-dimensional global simulation of multiple ICMEs' interaction and propagation from the Sun to the heliosphere following the 25–28 October 2003 solar events, *Adv. Space Res.*, *40*, 1827–1834.

Wu, C.-C., M. Dryer, S. T. Wu, B. E. Wood, C. D. Fry, K. Liou, and S. Plunkett (2011), Global three-dimensional simulation of the interplanetary evolution of the observed geoeffective coronal mass ejection during the epoch 1–4 August 2010, *J. Geophys. Res.*, *116*, A12103, doi:10.1029/2011JA016947.

Xie, H., L. Ofman, and G. Lawrence (2004), Cone model for halo CMEs: Applications to space weather forecasting, *J. Geophys. Res.*, *109*, A03109, doi:10.1029/2003JA010226.

Xie, H., N. Gopalswamy, L. Ofman, O. C. St. Cyr, G. Michalek, A. Lara, and S. Yashiro (2006), Improved input to the empirical coronal mass ejection (CME) driven shock arrival model from CME cone models, *Space Weather*, *4*, S10002, doi:10.1029/2006SW000227.

Yang, L. P., X. S. Feng, C. Q. Xiang, S. H. Zhang, and S. T. Wu (2011), Simulation of the unusual solar minimum with 3D SIP-CESE MHD Model by comparison with multi-satellite observations, *Sol. Phys.*, *271*, 91–110.

Yang, L. P., X. S. Feng, C. Q. Xiang, Y. Liu, X. Zhao, and S. T. Wu (2012), Time-dependent MHD modeling of the global solar corona for year 2007: Driven by daily-updated magnetic field synoptic data, *J. Geophys. Res.*, *117*, A08110, doi:10.1029/2011JA017494.

Zhang, J., K. P. Dere, R. A. Howard, and V. Bothmer (2003), Identification of solar sources of major geomagnetic storms between 1996 and 2000, *Astrophys. J.*, *582*, 520–533.

Zhao, X. H., and X. S. Feng (2014), Shock propagation model version-2 (SPM2) and its application in predicting the arrivals at Earth of interplanetary shocks during Solar Cycle 23, *J. Geophys. Res. Space Physics*, *119*, 1–10, doi:10.1002/2012JA018503.

Zhao, X. H., X. S. Feng, and C.-C. Wu (2007), Influence of solar flare's location and heliospheric current sheet on the associated shock's arrival at Earth, *J. Geophys. Res.*, *112*, A06107, doi:10.1029/2006JA012205.

Zhao, X. H., X. S. Feng, C. Q. Xiang, Y. Liu, Z. Li, Y. Zhang, and S. T. Wu (2010), Multi-spacecraft observations of the 2008 January 2 CME in the inner heliosphere, *Astrophys. J.*, *714*, 1133–1141.

Zhao, X. P., S. P. Plunkett, and W. Liu (2002), Determination of geometrical and kinematical properties of halo coronal mass ejections using the cone model, *J. Geophys. Res.*, *107*(A8), 1223, doi:10.1029/2001JA009143.

Zheng, Y. H., et al. (2013), Forecasting propagation and evolution of CMEs in an operational setting: What has been learned, *Space Weather*, *11*, 1–18, doi:10.1002/swe.20096.

Zhou, Y. F., X. S. Feng, S. T. Wu, D. Du, F. Shen, and C. Q. Xiang (2012), Using a 3-D spherical plasmoid to interpret the Sun-to-Earth propagation of the 4 November 1997 coronal mass ejection event, *J. Geophys. Res.*, *117*, A01102, doi:10.1029/2010JA016380.